Metrization and Simulation of Controlled Hybrid Systems

Samuel A. Burden, *Student, IEEE*, Humberto Gonzalez, *Member, IEEE*, Ramanarayan Vasudevan, *Member, IEEE*, Ruzena Bajcsy, *Fellow, IEEE*, and S. Shankar Sastry, *Fellow, IEEE*

Abstract

The study of controlled hybrid systems requires practical tools for approximation and comparison of system behaviors. Existing approaches to these problems impose undue restrictions on the system's continuous and discrete dynamics. Metrization and simulation of controlled hybrid systems is considered here in a unified framework by constructing a state space metric. The metric is applied to develop a numerical simulation algorithm that converges uniformly, with a known rate of convergence, to orbitally stable executions of controlled hybrid systems, up to and including Zeno events. Benchmark hybrid phenomena illustrate the utility of the proposed tools.

I. Introduction

For continuous–state dynamical systems and finite–state automata there exist rich sets of tools for metrization and simulation. The interaction of discrete transitions with continuous dynamics introduces subtleties that render the development of similar tools for controlled hybrid systems non-trivial. Consider the time evolution of a pair of states $(\xi_1, \xi_2) \in \mathbb{R}^2$. Suppose that when either quantity crosses zero a discontinuous change in the time derivatives $(\dot{\xi}_1, \dot{\xi}_2)$ is triggered yielding a discontinuous planar vector field as in Fig. 1a. A faithful model of the system's full state evolution is *hybrid*, representing both discrete and continuous state transitions, as in Fig. 1b.

The choice of metric for this controlled hybrid system dictates exactly the type of trajectories that can be faithfully simulated. For example, existing trajectory–space metrics impose at least unit distance between any states that reside in different discrete modes [1], [2], [3], [4]. As a result, simulation algorithms based on these metrics cannot provably approximate executions that undergo simultaneous discrete transitions (e.g. x) since nearby executions encounter different discrete transition sequences (e.g. y_δ, z_δ).

To overcome this limitation, we construct a distance metric over the state space of a controlled hybrid system and apply this metric to develop a provably–convergent numerical simulation algorithm applicable to the class of hybrid systems illustrated in Fig. 1b. Our framework enables formal investigation of a wide range of systems: the dynamics may be nonlinear, the continuous dynamics may be controlled, and multiple discrete transitions may occur simultaneously, so long as executions are orbitally stable.

Efforts to construct topologies on controlled hybrid systems have been significant, and can be best appreciated in this context by determining whether they induce a metric space. Nerode and Kohn [5] define state–space topologies that are not required to be metric spaces but are generated by finite–state automata associated with digital control systems. Simic et al. [6] apply a quotient construction to obtain, under regularity conditions, a topological manifold (or *hybrifold*). Ames and Sastry [7] derive a category–theoretic *colimit* topology over the *regularization* proposed by Johansson et al. [8] that relaxes domains at the guard sets. We propose a metric topology over the state space of controlled hybrid systems that connects disparate domains through the reset map, effectively metrizing the *hybrifold* and *colimit*

S. Burden was supported in part by an NSF Graduate Research Fellowship. Part of this research was sponsored by the Army Research Laboratory under Cooperative Agreement W911NF-08-2-0004.

S. Burden, R. Bajcsy, and S. S. Sastry are with the University of California at Berkeley, EECS Dept. Email: sburden,bajcsy,sastry@eecs.berkeley.edu.

H. Gonzalez is with the Washington University in St. Louis, ESE Dept. Email: hgonzale@ese.wustl.edu.

R. Vasudevan is with the Massachusetts Institute of Technology, CSAIL. Email: ramv@csail.mit.edu.

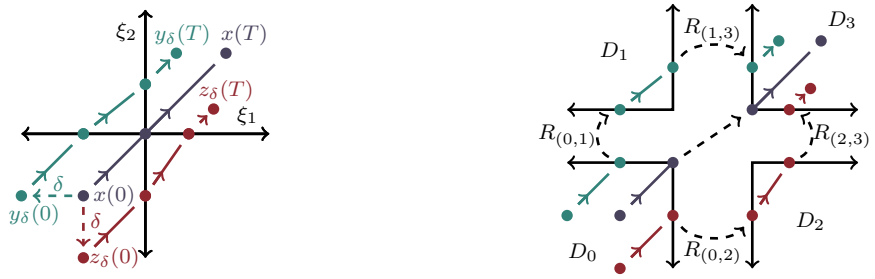

(a) digital control system (b) controlled hybrid system

Fig. 1. Illustration of digital control system governing the time evolution of two physical quantities $(\xi_1, \xi_2) \in \mathbb{R}^2$ (Fig. 1a) and a controlled hybrid system induced by discrete transitions in the digital controller state (Fig. 1b). The execution x undergoes two discrete transitions simultaneously; the nearby executions y_δ, z_δ encounter different discrete transition sequences. Since $R_{(1,3)} \circ R_{(0,1)}(0,0) = R_{(2,3)} \circ R_{(0,2)}(0,0) = (0,0)$, either transition sequence may be chosen for x.

topologies, and generalizing the *phase space* metric proposed by Schatzman for an impact oscillator [9]. In contrast, Tavernini [1] and Gobel and Teel [10] directly metrize the space of executions of hybrid systems; Gokhman [2] demonstrates the equivalence of the resulting topology with that generated by the Skorohod trajectory metric [11, Chapter 6]). We highlight in more detail the limitations imposed by metrizing the trajectory space rather than state space in Section V-A.

The literature on numerical simulation of hybrid systems may be partitioned into two groups: practical algorithms focused on high–precision estimates of discrete event times, and theoretical proofs of convergence for simulations. Practical algorithms aim to place time–steps close to discrete event times using root–finding [12], [13], [14]. Theoretical proofs of convergence have generally required restrictive assumptions: Esposito et al. [15], apply feedback linearization to asymptotically guarantee event detection for semi–algebraic guards, while Paoli and Schatzman [16] develop a provably–convergent algorithm for mechanical states undergoing impact. The most general convergence results relax the requirement that discrete transition times be determined accurately [1], [3], [4], [17], and consequently can accommodate arbitrary nonlinear transition surfaces, Lipschitz continuous vector fields, and continuous discrete transition maps. We extend this approach using our state–space metric to prove convergence, at least at a linear rate, to executions that satisfy an *orbital stability* property described in Section IV. Our algorithm is applicable to hybrid systems possessing control inputs and overlapping guards, representing a substantial contribution beyond our previous efforts [17] and those of others [1], [3], [4].

Organization: Section II contains definitions of mathematical concepts of interest. Section III contains our technique for metrization and relaxation of controlled hybrid systems. In Section IV we develop an algorithm for numerical simulation and prove uniform convergence at a linear rate of simulations to orbitally stable executions. The technical and practical advantages of our techniques are illustrated in a series of examples in Section V.

II. Preliminaries

We begin with the definitions and assumptions used throughout the paper.

A. Topology

The 2–norm is our finite–dimensional norm of choice unless otherwise specified. Let P_A be the set of all finite partitions of $A \subset \mathbb{R}$. Given $n \in \mathbb{N}$, we define the *total variation* of $f \in L^\infty(\mathbb{R}, \mathbb{R}^n)$ by:

$$\mathrm{V}(f) = \sup\left\{ \sum_{j=0}^{m-1} \|f(t_{j+1}) - f(t_j)\|_1 \,|\, \{t_k\}_{k=0}^m \in P_{\mathbb{R}}, m \in \mathbb{N} \right\}, \tag{1}$$

where $L^\infty(\mathbb{R},\mathbb{R}^n)$ is the set of all almost everywhere bounded functions from $\mathbb{R}$ to $\mathbb{R}^n$. The total variation of f is a semi–norm, i.e. it satisfies the Triangle Inequality, but does not separate points. f is of *bounded variation* if $\mathrm{V}(f)<\infty$, and we define $BV(\mathbb{R},\mathbb{R}^n)$ to be the set of all functions of bounded variation from $\mathbb{R}$ to $\mathbb{R}^n$.

Given $n\in\mathbb{N}$ and $D\subset\mathbb{R}^n$, ∂D is the boundary of D, and $\mathrm{int}(D)$ is the interior of D. Recall that given a collection of sets $\{S_\alpha\}_{\alpha\in\mathcal{A}}$, where $\mathcal{A}$ might be uncountable, the *disjoint union* of this collection is $\coprod_{\alpha\in\mathcal{A}} S_\alpha = \bigcup_{\alpha\in\mathcal{A}} S_\alpha\times\{\alpha\}$, a set that is endowed with the piecewise–defined topology. Throughout the paper we will abuse notation and say that given $\bar\alpha\in\mathcal{A}$ and $x\in S_{\bar\alpha}$, then $x\in\coprod_{\alpha\in\mathcal{A}} S_\alpha$, even though we should write $\iota_{\bar\alpha}(x)\in\coprod_{\alpha\in\mathcal{A}} S_\alpha$, where $\iota_{\bar\alpha}\colon S_{\bar\alpha}\to\coprod_{\alpha\in\mathcal{A}} S_\alpha$ is the *canonical identification* $\iota_{\bar\alpha}(x)=(x,\bar\alpha)$.

In this paper we make extensive use of the concept of a *quotient topology* induced by an equivalence relation defined on a topological space. We regard a detailed exposition of this important concept as outside the scope of this paper, and refer the reader to Chapter 3 in [18] or Section 22 in [19] for more details. The next definition formalizes equivalence relations in topological spaces induced by functions. If $f\colon A\to B$, $V\subset A$, and $V'\subset B$, then we let $f(V)=\{f(a)\in B\mid a\in V\}$ denote the image of V under f, and $f^{-1}(V')=\{a\in A\mid f(a)\in V'\}$ denote the pre–image of V under f.

Definition 1. *Let $\mathcal{S}$ be a topological space, $A,B\subset\mathcal{S}$ two subsets, and $f\colon A\to B$ a function. The* f–induced equivalence relation*, denoted Λ_f, is the smallest equivalence relation containing the set $\big\{(a,b)\in\mathcal{S}\times\mathcal{S}\mid a\in f^{-1}(b)\big\}$ (Section 4.2.4 in [20]). We say that $a,b\in\mathcal{S}$* are f–related*, denoted by $a\overset{f}{\sim}b$, if $(a,b)\in\Lambda_f$. Moreover, the* equivalence class of $x\in\mathcal{S}$ *is defined as $[x]_f=\Big\{a\in\mathcal{S}\mid a\overset{f}{\sim}x\Big\}$, and the set of equivalence classes is defined as $\frac{\mathcal{S}}{\Lambda_f}=\big\{[x]_f\mid x\in\mathcal{S}\big\}$. We endow the* quotient $\frac{\mathcal{S}}{\Lambda_f}$ *with the quotient topology.*

Note that Λ_f is reflexive, symmetric, and transitive, i.e. an equivalence relation. An important application of the function–induced quotient is the construction of a single topological space out of several disconnected sets. Indeed, given a collection of sets $\{S_\alpha\}_{\alpha\in\mathcal{A}}$, where $\mathcal{A}$ is some index set, and a function $f\colon U\to\coprod_{\alpha\in\mathcal{A}} S_\alpha$, where $U\subset\coprod_{\alpha\in\mathcal{A}} S_\alpha$, then $\widehat{S}=\frac{\coprod_{\alpha\in\mathcal{A}} S_\alpha}{\Lambda_f}$ is a topological space.

Next, we present a useful concept from graph theory that simplifies our ensuing analysis.

Definition 2. *Let $(\mathcal{J},\Gamma)$ be a directed graph, where $\mathcal{J}$ is the set of vertices and $\Gamma\subset\mathcal{J}\times\mathcal{J}$ is the set of edges. Then, given $j\in\mathcal{J}$, define the* neighborhood of j*, denoted $\mathcal{N}_j$, by:*

$$\mathcal{N}_j=\{e\in\Gamma\mid\exists j'\in\mathcal{J}\text{ such that }e=(j,j')\}. \tag{2}$$

B. Length Metrics

Every metric space has an induced length metric, defined by measuring the length of the shortest curve between two points. Throughout this paper, we use induced length metrics to metrize the function–induced quotients of disjoint unions of sets. To formalize this approach, we begin by defining the length of a curve in a metric space; the following definition is equivalent to Definition 2.3.1 in [21].

Definition 3. *Let (S,d) be a metric space, $I\subset[0,1]$ be an interval, and $\gamma\colon I\to\mathcal{S}$ be a continuous function. Define the* length of γ under the metric d *by:*

$$L_d(\gamma)=\sup\Bigg\{\sum_{i=0}^{k-1} d\big(\gamma(\bar t_i),\gamma(\bar t_{i+1})\big)\mid k\in\mathbb{N},\ \{\bar t_i\}_{i=0}^k\in P_I\Bigg\}. \tag{3}$$

We now define a generalization of continuous curves for quotiented disjoint unions.

Definition 4. *Let $\{S_\alpha\}_{\alpha\in\mathcal{A}}$ be a collection of sets and $f\colon U\to\coprod_{\alpha\in\mathcal{A}} S_\alpha$, where $U\subset\coprod_{\alpha\in\mathcal{A}} S_\alpha$. $\gamma\colon[0,1]\to\coprod_{\alpha\in\mathcal{A}} S_\alpha$ is* f–connected *if there exists $k\in\mathbb{N}$ and $\{t_i\}_{i=0}^k\subset[0,1]$ with $0=t_0\le t_1\le\ldots\le t_k=1$ such*

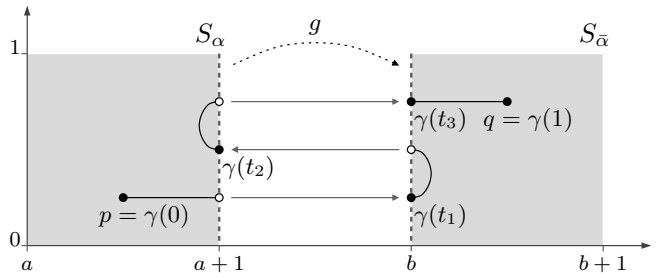

Fig. 2. g–connected curve γ with partition $\{t_i\}_{i=0}^4$, where $S_\alpha = [a, a+1] \times [0,1]$, $S_{\bar{\alpha}} = [b, b+1] \times [0,1]$, and $g\colon \{a+1\} \times [0,1] \to \{b\} \times [0,1]$ with $g(a+1, x) = (b, x)$.

that $\gamma|_{[t_i,t_{i+1})}$ is continuous for each $i \in \{0, 1, \ldots, k-2\}$, $\gamma|_{[t_{k-1},t_k]}$ is continuous, and $\lim_{t \uparrow t_i} \gamma(t) \overset{f}{\sim} \gamma(t_i)$ for each $i \in \{0, 1, \ldots, k-1\}$. Moreover, in that case $\{t_i\}_{i=0}^k$ is called a partition of γ.

Note that, since each section $\gamma|_{[t_i,t_{i+1})}$ is continuous, it must necessarily belong to a single set S_α for some $\alpha \in \mathcal{A}$ because the disjoint union is endowed with the piecewise–defined topology. In the case when $\mathcal{A} = \{\alpha\}$ is a singleton, then every id_{S_α}–connected curve is simply a continuous curve over S_α, where id_{S_α} denotes the identity function in S_α. Figure 2 shows an example of a connected curve over a collection of two sets.

Using the concept of connected curves, we now define the induced length distance of a collection of metric spaces. The induced length distance is a generalization of the induced metric defined in Chapter 2 in [21].

Definition 5. *Let $\{(S_\alpha, d_\alpha)\}_{\alpha \in \mathcal{A}}$ be a collection of metric spaces, and let $\{X_\alpha\}_{\alpha \in \mathcal{A}}$ be a collection of sets such that $X_\alpha \subset S_\alpha$ for each $\alpha \in \mathcal{A}$. Furthermore, let $f\colon U \to \coprod_{\alpha \in \mathcal{A}} X_\alpha$, where $U \subset \coprod_{\alpha \in \mathcal{A}} X_\alpha$, and let $\widehat{X} = \frac{\coprod_{\alpha \in \mathcal{A}} X_\alpha}{\Lambda_f}$. $\widetilde{d}_{\widehat{X}}\colon \widehat{X} \times \widehat{X} \to [0, \infty]$ is the f–*induced* length distance of $\widehat{X}$, defined by:*

$$\widetilde{d}_{\widehat{X}}(p,q) = \inf\Bigg\{ \sum_{i=0}^{k-1} L_{d_{\alpha_i}}\big(\gamma|_{[t_i,t_{i+1})}\big) \mid \gamma\colon [0,1] \to \coprod_{\alpha \in \mathcal{A}} X_\alpha, \gamma(0) = p,\ \gamma(1) = q, \\ \gamma \text{ is } f\text{–connected},\ \{t_i\}_{i=0}^k \in P_{[0,1]},\ \{\alpha_i\}_{i=0}^{k-1} \text{ s.t. } \gamma\big([t_i, t_{i+1})\big) \subset X_{\alpha_i}\ \forall i \Bigg\}. \quad (4)$$

We invoke this definition to metrize both subsets and disjoint unions of metric spaces. It is important to note that although $\widetilde{d}_{\widehat{X}}$ is non–negative, symmetric, and subadditive, it does not necessarily separate points of $\widehat{X}$ (see Section 2.3 in [21]), and hence generally only defines a *pseudo*–metric. In the special case where no function f is supplied, then by convention we let $f = \mathrm{id}_X$, the identity function on X. This implies $\widehat{X} = X$ and the induced metric coincides with the given metric. The following Lemma is a straightforward consequence of Proposition 2.3.12 in [21].

Lemma 6. *Let (S, d) be a metric space and $X \subset S$. Then $\widetilde{d}_X$ is a metric. Moreover, the topology on X induced by $\widetilde{d}_X$ is equivalent to the topology on X induced by d.*

C. Controlled Hybrid Systems

Motivated by the definition of hybrid systems presented in [6], we define the class of hybrid systems of interest in this paper.

Definition 7. *A* controlled hybrid system *is a tuple*

$$\mathcal{H} = (\mathcal{J}, \Gamma, \mathcal{D}, U, \mathcal{F}, \mathcal{G}, \mathcal{R}), \quad (5)$$

where:

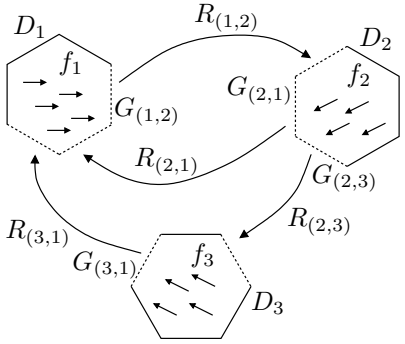

Fig. 3. Illustration of a controlled hybrid system with three modes.

- *$\mathcal{J}$ is a finite set indexing the discrete states of $\mathcal{H}$;*
- *$\Gamma \subset \mathcal{J} \times \mathcal{J}$ is the set of edges, forming a directed graph structure over $\mathcal{J}$;*
- *$\mathcal{D} = \{D_j\}_{j\in\mathcal{J}}$ is the set of domains, where each D_j is a subset of $\mathbb{R}^{n_j}$, $n_j \in \mathbb{N}$;*
- *$U \subset \mathbb{R}^m$ is the range space of control inputs, $m \in \mathbb{N}$;*
- *$\mathcal{F} = \{f_j\}_{j\in\mathcal{J}}$ is the set of vector fields, where each $f_j \colon \mathbb{R} \times D_j \times U \to \mathbb{R}^{n_j}$ is the vector field defining the dynamics of the system on D_j;*
- *$\mathcal{G} = \{G_e\}_{e\in\Gamma}$ is the set of guards, where each $G_{(j,j')} \subset \partial D_j$ is a guard in mode $j \in \mathcal{J}$ that defines a transition to mode $j' \in \mathcal{J}$; and,*
- *$\mathcal{R} = \{R_e\}_{e\in\Gamma}$ is the set of reset maps, where each map $R_{(j,j')} \colon G_{(j,j')} \to D_{j'}$ defines the transition from guard $G_{(j,j')}$.*

For convenience, we sometimes refer to controlled hybrid systems as just hybrid systems, and we refer to the distinct vertices within the graph structure associated with a controlled hybrid system as modes. Each domain in the definition of a controlled hybrid system is a metric space with the Euclidean distance metric. A three–mode autonomous hybrid system, which is a particular case of Definition 7 where none the vector fields $\{f_j\}_{j\in\mathcal{J}}$ depend on the control input, is illustrated in Fig. 3. Note that we restrict control inputs to the continuous flow, hence inputs do not have an effect during discrete transitions.

Next, we impose several technical assumptions that support existence and uniqueness of executions on hybrid domains. We delay the definition of executions of a hybrid system to Section IV-A once all the technical details regarding the metrization of spaces have been presented.

Assumption 8. *Let $\mathcal{H}$ be a controlled hybrid system. Then the following statements are true:*
(1) For each $j \in \mathcal{J}$, D_j is a compact n_j–dimensional manifold with boundary.
(2) U is compact.
(3) For each $e \in \Gamma$, G_e is a closed, embedded, codimension 1 submanifold with boundary.
(4) For each $e \in \Gamma$, R_e is continuous.

Assumption 9. *For each $j \in \mathcal{J}$, f_j is Lipschitz continuous. That is, there exists $L > 0$ such that for each $j \in \mathcal{J}$, $t_1, t_2 \in \mathbb{R}$, $x_1, x_2 \in D_j$, and $u_1, u_2 \in U$:*

$$\big\| f_j(t_1, x_1, u_1) - f_j(t_2, x_2, u_2) \big\| \leq L\big(|t_1 - t_2| + \|x_1 - x_2\| + \|u_1 - u_2\|\big). \tag{6}$$

Assumption 9 guarantees the existence and uniqueness of solutions to ordinary differential equations in individual domains. In the sequel we will consider control inputs of *bounded variation* $u \in BV(\mathbb{R}, U)$. Note that without loss of generality we take 0 as the initial time in the following Lemma; a general initial time can be accommodated by a straightforward change of variables.

Lemma 10. *Let $\mathcal{H}$ be a controlled hybrid system. Then for each $j \in \mathcal{J}$, each initial condition $p \in D_j$, and each control $u \in BV(\mathbb{R}, U)$, there exists an interval $I \subset \mathbb{R}$ with $0 \in I$ such that the following differential*

equation has a unique solution:

$$\dot{x}(t) = f_j\big(t, x(t), u(t)\big), \quad t \in I, \quad x(0) = p. \tag{7}$$

x is called the integral curve *of f_j with initial condition p and control u. Moreover, $x|_I$ is absolutely continuous.*

Proof. Let $\widetilde{f}_j \colon \mathbb{R} \times \mathbb{R}^{n_j} \times U \to \mathbb{R}^{n_j}$ be any globally Lipschitz continuous extension to f_j (guaranteed to exist by Theorem 1 in [22]). Given any $p \in D_j \subset \mathbb{R}^{n_j}$ and $u \in BV(\mathbb{R}, U)$, Proposition 5.6.5 in [23] guarantees the existence of an integral curve $\widetilde{x} \colon \widetilde{I} \to \mathbb{R}^{n_j}$ for $\widetilde{f}_j$ with initial condition $\widetilde{x}(0) = p$. Note that $\widetilde{x}$ is absolutely continuous by Theorem 3.35 in [24]. Let $I \subset \widetilde{I}$ be the connected component of $\widetilde{x}^{-1}(D_j)$ containing 0. Then $x = \widetilde{x}|_I$ is an absolutely continuous integral curve of f_j and $x(I) \subset D_j$. Note that x is unaffected by the choice of extension $\widetilde{f}_j$. □

The following definition is used to construct executions of a controlled hybrid system.

Definition 11. *Let $\mathcal{H}$ be a controlled hybrid system, $j \in \mathcal{J}$, $p \in D_j$, and $u \in BV(\mathbb{R}, U)$. $x \colon I \to D_j$ is the* maximal integral curve *of f_j with initial condition p and control u if, given any other integral curve with initial condition p and control u, such as $\tilde{x} \colon \widetilde{I} \to D_j$, then $\widetilde{I} \subset I$.*

Given a maximal integral curve $x \colon I \to D_j$, a direct consequence[1] of Definition 11 and Assumption 8 is that either $\sup I = +\infty$, or $\sup I = t' < \infty$ and $x(t') \in \partial D_j$. This fact is critical during the definition of executions of a controlled hybrid systems in Section IV.

III. Metrization and Relaxation of Controlled Hybrid Systems

In this section, we metrize a unified family of spaces containing all the domains of a controlled hybrid system $\mathcal{H}$. The constructed metric space has three appealing properties: first, the distance between a point in a guard and its image via its respective reset map is zero; second, the distance between points in different domains are properly defined and finite; and third, the distance between points is based on the Euclidean distance metric from each domain.

A. Hybrid Quotient Space

Using Definitions 5 and 7, we construct a metric space where the executions of a controlled hybrid system reside. The result is a metrization of the *hybrifold* [6].

Definition 12. *Let $\mathcal{H}$ be a controlled hybrid system, and let*

$$\widehat{R} \colon \coprod_{e \in \Gamma} G_e \to \coprod_{j \in \mathcal{J}} D_j \tag{8}$$

be defined by $\widehat{R}(p) = R_e(p)$ for each $p \in G_e$. Then the hybrid quotient space *of $\mathcal{H}$ is:*

$$\mathcal{M} = \frac{\coprod_{j \in \mathcal{J}} D_j}{\Lambda_{\widehat{R}}}. \tag{9}$$

Fig. 4 illustrates the construction in Definition 12. The induced length distance on $\mathcal{M}$ is in fact a distance metric:

Theorem 13. *Let $\mathcal{H}$ be a controlled hybrid system, and let $\widetilde{d}_{\mathcal{M}}$ be the $\widehat{R}$–induced length distance of $\mathcal{M}$, where $\widehat{R}$ is defined in* (8)*. Then $\widetilde{d}_{\mathcal{M}}$ is a metric on $\mathcal{M}$, and the topology it induces is equivalent to the $\widehat{R}$–induced quotient topology.*

[1]This follows from continuity of integral curves and compactness of hybrid domains.

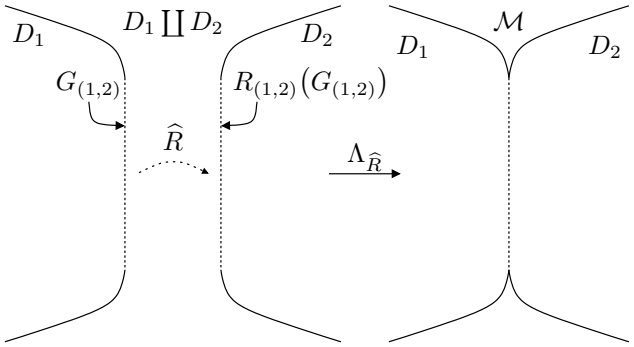

Fig. 4. The disjoint union of D_1 and D_2 (left) and the hybrid quotient space $\mathcal{M}$ obtained from the relation $\Lambda_{\widehat{R}}$ (right).

Proof. We provide the main arguments of the proof, omitting the details in the interest of brevity. First, note that each domain is a normal space, i.e. every pair of disjoint closed sets have disjoint neighborhoods. Second, note that each reset map is a closed map, i.e. the image of closed sets under the reset map are closed. This fact follows by Condition (3) in Assumption 8, since each guard is compact, thus reset maps are closed by the Closed Map Lemma (Lemma A.19 in [25]).

Let $\widehat{D} = \coprod_{j \in \mathcal{J}} D_j$ and $p, q \in \widehat{D}$. We aim to show that if p and q yield distinct equivalence classes (i.e. $(p,q) \notin \Lambda_{\widehat{R}}$) then the induced distance between them is strictly positive. Note that the equivalence classes $[p]_{\widehat{R}}$ and $[q]_{\widehat{R}}$ are each a finite collection of closed sets. Moreover, since we can construct disjoint neighborhoods around each of these closed sets, then we can conclude that there exists $\delta > 0$ such that $\widetilde{d}_{\mathcal{M}}\big([p]_{\widehat{R}}, [q]_{\widehat{R}}\big) > \delta$. The proof concludes by following the argument in Exercise 3.1.14 in [21], i.e. since each connected component in $\widehat{D}$ is bounded, then $\mathcal{M}$ is also bounded (in the quotient topology). Then, using a simple extension of Theorem 5.8 in [18][2], we get that the identity map from $\mathcal{M}$ to the space constructed by taking the quotient of all the points in $\widehat{D}$ such that $\widetilde{d}_{\mathcal{M}}$ has zero distance is a homeomorphism, thus they have the same topology. □

It is crucial to note that all $\widehat{R}$–connected curves are continuous in the topology induced by the metric $\widetilde{d}_{\mathcal{M}}$ on the hybrid quotient space $\mathcal{M}$. This implies in particular that executions of controlled hybrid systems (to be defined in Section IV) are continuous in $\mathcal{M}$ since the endpoint of the segment of an execution that lies in a guard G_e will be $\widehat{R}$–related to the startpoint of the subsequent segment of the execution; alternately, this follows from Theorem 3.12(b) in [6] since $\mathcal{M}$ is equivalent to the "hybrifold" construction in that paper. This important property is foundational to the convergence results for sequences of (relaxed) executions and their simulations derived in Section IV. For further details, we refer the interested reader to Examples 3.2 and 3.3 in [6] where continuity is clearly discussed for simple examples.

B. Relaxation of a Controlled Hybrid System

To construct a numerical simulation scheme that does not require the exact computation of the time instant when an execution intersects a guard, we require a method capable of introducing some slackness within the computation. This is accomplished by relaxing[3] each domain along its guard and then relaxing each vector field and reset map accordingly in order to define a relaxation of a controlled hybrid system.

To formalize this approach, we begin by defining the relaxation of each domain of a controlled hybrid system, which is accomplished by first attaching an ε–sized strip to each guard.

[2]The extension aims to allow the domain of the map to be bounded instead of compact. The new proof follows step–by–step the argument in [18].

[3]This should not be confused with the "relaxation" of hybrid inclusions described by Cai et al. [26]. Since interpreting our controlled hybrid systems as hybrid inclusions yields singleton–valued "flow" and "jump" maps, relaxation in this sense does not yield a distinct hybrid system.

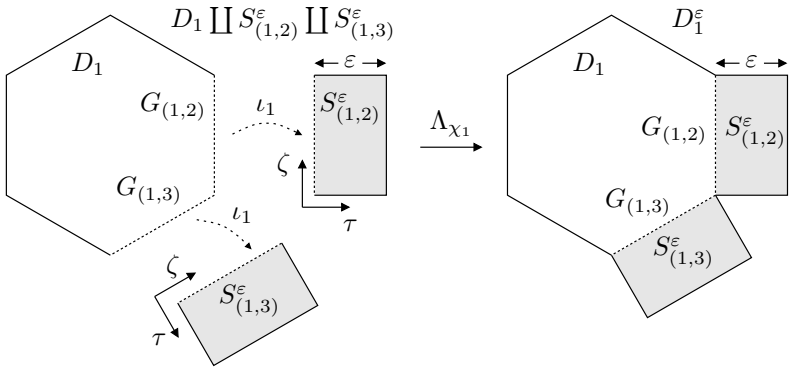

Fig. 5. Disjoint union of D_1 and the strips in its neighborhood, $\{S^\varepsilon_e\}_{e\in\mathcal{N}_1}$ (left), and the relaxed domain D^ε_1 obtained from the relation Λ_{χ_1} (right).

Definition 14. *Let $\mathcal{H}$ be a controlled hybrid system. For each $e \in \Gamma$, let $S^\varepsilon_e = G_e \times [0,\varepsilon]$ be the* strip associated to guard G_e. *For each $j \in \mathcal{J}$, let*

$$\chi_j \colon \coprod_{e\in\mathcal{N}_j} G_e \to \coprod_{e\in\mathcal{N}_j} S^\varepsilon_e, \tag{10}$$

be the canonical identification *of each point in a guard with its corresponding strip defined for each $p \in G_e$ as $\chi_j(p) = (p,0) \in S^\varepsilon_e$. Then, the* relaxation of D_j *is defined by:*

$$D^\varepsilon_j = \frac{D_j \coprod \left(\coprod_{e\in\mathcal{N}_j} S^\varepsilon_e\right)}{\Lambda_{\chi_j}}. \tag{11}$$

By Condition (3) in Assumption 8, each point on a strip S^ε_e of D_j is defined using n_j coordinates $(\zeta_1,\ldots,\zeta_{n_j-1},\tau)$, shortened (ζ,τ), where τ is called the *transverse coordinate* and is the distance along the interval $[0,\varepsilon]$. An illustration of Definition 14 together with the coordinates on each strip is shown in Fig. 5.

We endow each S^ε_e with a distance metric in order to define an induced length metric on a relaxed domain D^ε_j.

Definition 15. *Let $j \in \mathcal{J}$ and $e \in \mathcal{N}_j$. Endow D_j with $\widetilde{d}_{D_j}$ as its metric, and $d_{S^\varepsilon_e} \colon S^\varepsilon_e \times S^\varepsilon_e \to [0,\infty)$ as the metric on S^ε_e, defined for each $\zeta,\zeta' \in G_e$ and $\tau,\tau' \in [0,\varepsilon]$ by:*

$$d_{S^\varepsilon_e}\big((\zeta,\tau),(\zeta',\tau')\big) = \widetilde{d}_{G_e}(\zeta,\zeta') + |\tau-\tau'|. \tag{12}$$

We now define a length metric on relaxed domains using Definitions 4 and 5.

Theorem 16. *Let $j \in \mathcal{J}$, and let $\widetilde{d}_{D^\varepsilon_j}$ be the χ_j–induced length distance on D^ε_j, where χ_j is as defined in* (10)*. Then $\widetilde{d}_{D^\varepsilon_j}$ is a metric on D^ε_j, and the topology it induces is equivalent to the χ_j–induced quotient topology.*

Proof. Since $\widetilde{d}_{D^\varepsilon_j}$ is non–negative, symmetric, and subadditive, it remains to show that it separates points. Let $p,q \in D^\varepsilon_j$. First, we want to show that $[p]_{\chi_j} = [q]_{\chi_j}$ whenever $\widetilde{d}_{D^\varepsilon_j}(p,q) = 0$. Note that for each $e \in \mathcal{N}_j$ and each pair $p,q \in G_e$, and by the Definition 5 and 15, $d_{S^\varepsilon_e}((p,0),(q,0)) \geq \widetilde{d}_{D_j}(p,q)$, hence no connected curve that transitions to a strip can be shorter than a curve that stays in D_j. This fact immediately shows that for $p,q \in D_j$, $\widetilde{d}_{D^\varepsilon_j}(p,q) = 0$ implies that $[p]_{\chi_j} = [q]_{\chi_j}$. The case when one of the points is in $G_e \times (0,\varepsilon] \subset S^\varepsilon_e$ follows easily by noting that those points can be separated by a suitably–sized $d_{S^\varepsilon_e}$–ball. The proof concludes by following the argument in Exercise 3.1.14 in [21], as we did in the proof of Theorem 13. □

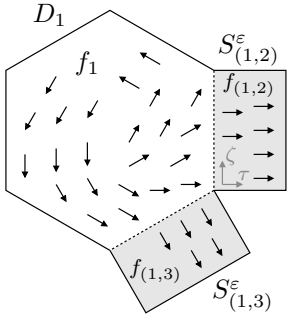

Fig. 6. Relaxed vector field f_1^ε on D_1^ε.

Refer to $\widetilde{d}_{D_j^\varepsilon}$ as the *relaxed domain metric*. Note that Theorem 16 can be proved using essentially the same argument as in the proof of Theorem 13, but we prove Theorem 16 to emphasize the utility of the inequality relating the induced metric on a domain and the metric on each strip.

Next, we define a vector field over each relaxed domain.

Definition 17. *Let $j \in \mathcal{J}$. For each $e \in \mathcal{N}_j$, let the vector field on the strip S_e^ε, denoted f_e, be the unit vector pointing outward along the transverse coordinate. In coordinates, $f_e\big(t,(\zeta,\tau),u\big) = \big(\underbrace{0,\ \ldots,\ 0}_{\zeta \text{ coords.}},\ 1\big)^T$. Then, the* relaxation of f_j *is:*

$$f_j^\varepsilon(t,x,u) = \begin{cases} f_j(t,x,u) & \text{if } x \in D_j, \\ f_e(t,x,u) & \text{if } x \in G_e \times (0,\varepsilon] \subset S_e^\varepsilon,\ e \in \mathcal{N}_j. \end{cases} \tag{13}$$

Note that the relaxation of the vector field is generally not continuous along each G_e, for $e \in \mathcal{N}_j$. As we show in the algorithm in Fig. 10, this discontinuous vector field does not lead to sliding modes on the guards [27], [28], since the vector field on the strips always points away from the guard. An illustration of the relaxed vector field f_j^ε on D_j^ε is shown in Fig. 6.

The definitions of relaxed domains and relaxed vector fields allow us to construct a relaxation of the controlled hybrid systems as follows:

Definition 18. *Let $\mathcal{H}$ be a controlled hybrid system. We say that the relaxation of $\mathcal{H}$ is a tuple:*

$$\mathcal{H}^\varepsilon = (\mathcal{J}, \Gamma, \mathcal{D}^\varepsilon, U, \mathcal{F}^\varepsilon, \mathcal{G}^\varepsilon, \mathcal{R}^\varepsilon), \tag{14}$$

where:

- $\mathcal{D}^\varepsilon = \big\{D_j^\varepsilon\big\}_{j\in\mathcal{J}}$ *is the set of relaxations of the domains in $\mathcal{D}$, and each D_j^ε is endowed with its induced length distance metric $\widetilde{d}_{D_j^\varepsilon}$;*
- $\mathcal{F}^\varepsilon = \big\{f_j^\varepsilon\big\}_{j\in\mathcal{J}}$ *is the set of relaxations of the vector fields in $\mathcal{F}$;*
- $\mathcal{G}^\varepsilon = \big\{G_e^\varepsilon\big\}_{e\in\Gamma}$ *is the set of relaxations of the guards in $\mathcal{G}$, where $G_e^\varepsilon = G_e \times \{\varepsilon\} \subset S_e^\varepsilon$ for each $e \in \Gamma$; and,*
- $\mathcal{R}^\varepsilon = \big\{R_e^\varepsilon\big\}_{e\in\Gamma}$ *is the set of relaxations of the reset maps in $\mathcal{R}$, where $R_e^\varepsilon \colon G_e^\varepsilon \to D_{j'}$ for each $e = (j,j') \in \Gamma$ and $R_e^\varepsilon(\zeta,\varepsilon) = R_e(\zeta)$ for each $\zeta \in G_e$.*

C. Relaxed Hybrid Quotient Space

Analogous to the construction of the metric quotient space $\mathcal{M}$, using Definitions 5 and 18 we construct a unified metric space where executions of relaxations of controlled hybrid systems reside. The result is a metrization of the *hybrid colimit* [7] (rather than a metrization of the hybrifold as in the previous section).

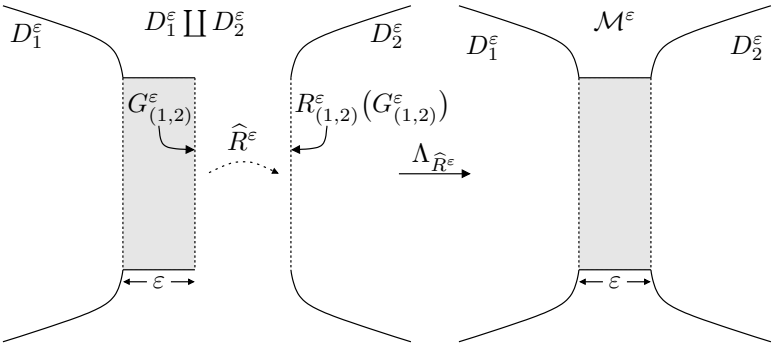

Fig. 7. The disjoint union of D_1^ε and D_2^ε (left), and the relaxed hybrid quotient space $\mathcal{M}^\varepsilon$ obtained from the relation $\Lambda_{\widehat{R}^\varepsilon}$ (right).

Definition 19. *Let $\mathcal{H}^\varepsilon$ be the relaxation of the controlled hybrid system $\mathcal{H}$. Also, let*

$$\widehat{R}^\varepsilon \colon \coprod_{e\in\Gamma} G_e^\varepsilon \to \coprod_{j\in\mathcal{J}} D_j^\varepsilon \tag{15}$$

be defined by $\widehat{R}^\varepsilon(p) = R_e^\varepsilon(p)$ for each $p \in G_e^\varepsilon$. Then the relaxed hybrid quotient space *of $\mathcal{H}^\varepsilon$ is:*

$$\mathcal{M}^\varepsilon = \frac{\coprod_{j\in\mathcal{J}} D_j^\varepsilon}{\Lambda_{\widehat{R}^\varepsilon}}. \tag{16}$$

The construction in Definition 19 is illustrated in Fig. 7.

We now show that the induced length distance on $\mathcal{M}^\varepsilon$ is indeed a metric. We omit this proof since it is identical to the proof of Theorem 13.

Theorem 20. *Let $\mathcal{H}$ be a controlled hybrid system, let $\mathcal{H}^\varepsilon$ be its relaxation, and let $\widetilde{d}_{\mathcal{M}^\varepsilon}$ be the $\widehat{R}^\varepsilon$–induced length distance of $\mathcal{M}^\varepsilon$, where $\widehat{R}^\varepsilon$ is defined in* (15)*. Then $\widetilde{d}_{\mathcal{M}^\varepsilon}$ is a metric on $\mathcal{M}^\varepsilon$, and the topology it induces is equivalent to the $\widehat{R}^\varepsilon$–induced quotient topology.*

All $\widehat{R}^\varepsilon$–connected curves are continuous under the metric topology induced by $\widetilde{d}_{\mathcal{M}^\varepsilon}$ which will be important when we study executions of hybrid systems in Section IV.

As expected, the metric on $\mathcal{M}^\varepsilon$ converges pointwise to the metric on $\mathcal{M}$.

Theorem 21. *Let $\mathcal{H}$ be a controlled hybrid system, and let $\mathcal{H}^\varepsilon$ be its relaxation. Then for each $p, q \in \mathcal{M}$, $\widetilde{d}_{\mathcal{M}^\varepsilon}(p,q) \to \widetilde{d}_{\mathcal{M}}(p,q)$ as $\varepsilon \to 0$.*

Proof. Abusing notation, let $L(\gamma)$ denote the length of any connected curve γ, defined as the sum of the lengths of each of its continuous sections under the appropriate metric. First, note that $\widetilde{d}_{\mathcal{M}}(p,q) \leq \widetilde{d}_{\mathcal{M}^\varepsilon}(p,q)$. This inequality follows since, as we argued in the proof of Theorem 16, given an edge $(j,j') \in \Gamma$, $d_{S^\varepsilon_{(j,j')}}\big((p',0),(q',0)\big) \geq \widetilde{d}_{D_j}(p',q')$ for any pair of points $p', q' \in G_{(j,j')}$. Thus, adding the strips $\{S_e\}_{e\in\Gamma}$ in $\mathcal{M}^\varepsilon$ only make the length of a connected curve longer.

Now let $\widehat{D} = \coprod_{j\in\mathcal{J}} D_j$ and $\widehat{D}^\varepsilon = \coprod_{j\in\mathcal{J}} D_j^\varepsilon$. Given $\delta > 0$, there exists $\gamma\colon [0,1] \to \widehat{D}$, an $\widehat{R}$–connected curve with partition $\{t_i\}_{i=0}^k$, such that $\gamma(0) = p$, $\gamma(1) = q$, and $\widetilde{d}_{\mathcal{M}}(p,q) \leq L(\gamma) \leq \widetilde{d}_{\mathcal{M}}(p,q) + \delta$. Moreover, without loss of generality let $\gamma^\varepsilon\colon [0,1] \to \widehat{D}^\varepsilon$ be an $\widehat{R}^\varepsilon$–connected curve that agrees with γ on $\widehat{D}$, i.e. each section of γ^ε on $\widehat{D}$ is identical, up to time scaling, to a section of γ. Thus γ^ε has at most k ε–length extra sections, $L(\gamma) \leq L(\gamma^\varepsilon) \leq L(\gamma) + k\varepsilon$, and $\widetilde{d}_{\mathcal{M}^\varepsilon}(p,q) \leq L(\gamma^\varepsilon) \leq \widetilde{d}_{\mathcal{M}}(p,q) + k\varepsilon + \delta$. But this inequality is valid for each $\delta > 0$, hence $\widetilde{d}_{\mathcal{M}^\varepsilon}(p,q) \leq \widetilde{d}_{\mathcal{M}}(p,q) + k\varepsilon$. The result follows after taking the limit as $\varepsilon \to 0$. □

Note that Theorem 21 does not imply that the topology of $\mathcal{M}^\varepsilon$ converges to the topology of $\mathcal{M}$. On the contrary, $\mathcal{M}^\varepsilon$ is homotopically equivalent to the graph $(\mathcal{J}, \Gamma)$ for each $\varepsilon > 0$ [7], whereas the topology of $\mathcal{M}$ may be different [6].

Require: $t = 0$, $j \in \mathcal{J}$, $p \in D_j$, and $u \in BV(\mathbb{R}, U)$.

1: Set $x(0) = p$.
2: **loop**
3: Let $\gamma\colon I \to D_j$ be the maximal integral curve of f_j with control u such that $\gamma(t) = x(t)$.
4: Let $t' = \sup I$ and $x(s) = \gamma(s)\ \forall s \in [t, t')$.
▷ *Note if* $t' < \infty$, *then* $\gamma(t') \in \partial D_j$.
5: **if** $t' = \infty$, **or** $\nexists e \in \mathcal{N}_j$ such that $\gamma(t') \in G_e$ **then**
6: Stop.
7: **end if**
8: Let $(j, j') \in \mathcal{N}_j$ be such that $\gamma(t') \in G_{(j,j')}$.
9: Set $x(t') = R_{(j,j')}\big(\gamma(t')\big)$, $t = t'$, and $j = j'$.
▷ *Note* $\gamma(t') \overset{\widehat{R}}{\sim} x(t')$.
10: **end loop**

Fig. 8. Algorithm to construct an execution of a controlled hybrid system $\mathcal{H}$.

We conclude this section by introducing metrics between curves on $\mathcal{M}^\varepsilon$.

Definition 22. *Let $I \subset [0, \infty)$ a bounded interval. Given any two curves $\gamma, \gamma'\colon I \to \mathcal{M}^\varepsilon$, we define:*

$$\rho_I^\varepsilon\big(\gamma, \gamma'\big) = \sup\big\{\widetilde{d}_{\mathcal{M}^\varepsilon}\big(\gamma(t), \gamma'(t)\big) \mid t \in I\big\}. \tag{17}$$

Our choice of the supremum among point–wise distances in Definition 22 is inspired by the sup–norm for continuous real–valued functions.

IV. Relaxed Executions and Discrete Approximations

This section contains our main result: discrete approximations of executions of controlled hybrid systems, constructed using any variable step size numerical integration algorithm, converge uniformly to the actual executions. This section is divided into three parts. First, we define a pair of algorithms that construct executions of controlled hybrid systems and their relaxations, respectively. Next, we develop a discrete approximation scheme for executions of relaxations of controlled hybrid systems. Finally, we prove that these discrete approximations converge to orbitally stable executions of the original, non–relaxed, controlled hybrid system using the metric topologies developed in Section III.

A. Execution of a Hybrid System

We begin by defining an *execution* of a controlled hybrid system. This definition agrees with the traditional intuition about executions of controlled hybrid systems which describes an execution as evolving as a standard control system until a guard is reached, at which point a discrete transition occurs to a new domain using a reset map. We provide an explicit definition to clarify technical details required in the proofs below. Given a controlled hybrid system, $\mathcal{H}$, as in Definition 7, the algorithm in Fig. 8 defines an execution of $\mathcal{H}$ via construction. A resulting execution, denoted x, is an $\widehat{R}$–connected curve from some interval $I \subset [0, \infty)$ to $\coprod_{j \in \mathcal{J}} D_j$. Thus, abusing notation, we regard x as a continuous curve on $\mathcal{M}$. Abusing notation again, we regard x as a piece–wise continuous curve on $\mathcal{M}^\varepsilon$ for each $\varepsilon > 0$. Fig. 9a shows an execution undergoing a discrete transition.

Note that executions constructed using the algorithm in Fig. 8 are not necessarily unique. Indeed, Definition 11 implies that once a discrete transition has been performed, the execution is unique until a new transition is made; however, the choice in Step 8 is not necessarily unique if the maximal integral curve passes through the intersection of multiple guards. It is not hard to prove that a sufficient condition for uniqueness of executions is that all the guards are disjoint, even though, as we show in Section V-C, uniqueness of the executions can be obtained for some cases where guards do intersect.

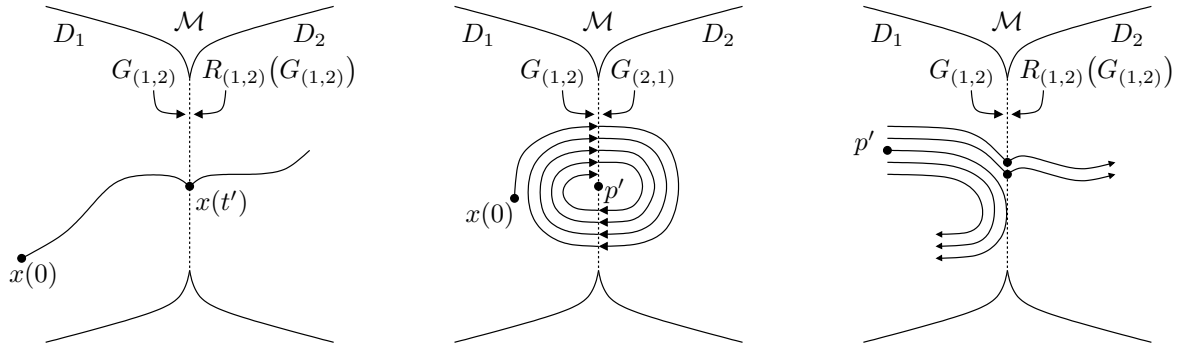

(a) Discrete transition of an execution x.

(b) Zeno execution x accumulating at p'.

(c) Non–orbitally stable execution at initial condition p'.

Fig. 9. Examples of different executions for a two–mode hybrid system.

With the definition of execution of a controlled hybrid system, we can define a class of executions unique to controlled hybrid systems.

Definition 23. *An execution is* Zeno *when it undergoes an infinite number of discrete transitions in a finite amount of time. Hence, there exists $T > 0$, called the* Zeno time*, such that the execution is only defined on $I = [0, T)$.*

Zeno executions are hard to simulate since they apparently require an infinite number of reset map evaluations, an impossible task to implement on a digital computer. A consequence of the algorithm in Fig. 8 is that if $x\colon I \to \mathcal{M}$ is an execution such that $T = \sup I < \infty$, then either

(1) x has a finite number of discrete transitions on $I = [0, T]$, and $x(T) \in \partial D_j$ for some $j \in \mathcal{J}$, or
(2) x is a Zeno execution and $I = [0, T)$.

We now introduce a property of Zeno executions of particular interest in this paper:

Definition 24. *Let $\mathcal{H}$ be a controlled hybrid system, $p \in \mathcal{M}$, $u \in BV(\mathbb{R}, U)$, and $x\colon [0, T) \to \mathcal{M}$ be a Zeno execution with initial condition p, control u, and Zeno time T.* x accumulates at $p' \in \mathcal{M}$ *if* $\lim_{t\to T} \widetilde{d}_{\mathcal{M}}\big(x(t), p'\big) = 0$.

Examples of Zeno executions that do not accumulate can be found in [29]. Fig. 9b shows a Zeno execution that accumulates at p'. Note that for p' to be a Zeno accumulation point, it must belong to a guard of a controlled hybrid system.

Since $\mathcal{M}$ is a metric space, we can introduce the concept of continuity of a hybrid execution with respect to its initial condition and control input in a straightforward way. Employing this definition, we can define the class of executions that are numerically approximable:

Definition 25. *Let $\mathcal{H}$ be a controlled hybrid system. Denote by $x_{(p,u)}\colon I_{(p,u)} \to \mathcal{M}$ a hybrid execution of $\mathcal{H}$ with initial condition $p \in \mathcal{M}$ and control $u \in BV(\mathbb{R}, U)$. Given $T > 0$, we say that $x_{(p,u)}$ is* orbitally stable in $[0, T]$ at (p, u) *if there exists a neighborhood of (p, u), say $N_{(p,u)} \subset \mathcal{M} \times BV(\mathbb{R}, U)$, such that:*

(1) $x_{(p',u')}$ is unique for each $(p', u') \in N_{(p,u)}$.
(2) $[0, T] \subset I_{(p',u')}$ for each $(p', u') \in N_{(p,u)}$.
(3) The map $(p', u') \mapsto x_{(p',u')}(t)$ is continuous at (p, u) for each $t \in [0, T]$.

As observed in Section III.B in [30], executions that are not orbitally stable are difficult to approximate with a general algorithm. Figure 9c shows a non–orbitally stable execution that intersects the guard tangentially, and note that executions initialized arbitrarily close to $p' \in D_1$ undergo different sequences of transitions. Unfortunately, there is presently no general test (analytical or numerical) that ensures a

Require: $t = 0$, $j \in \mathcal{J}$, $p \in D_j$, and $u \in BV(\mathbb{R}, U)$.
1: Set $x^\varepsilon(0) = p$.
2: **loop**
3: Let $\gamma\colon I \to D_j$, the maximal integral curve of f_j with control u such that $\gamma(t) = x^\varepsilon(t)$.
4: Let $t' = \sup I$ and $x^\varepsilon(s) = \gamma(s)\ \forall s \in [t, t')$.
▷ *Note if* $t' < \infty$, *then* $\gamma(t') \in \partial D_j$.
5: **if** $t' = \infty$, **or** $\nexists e \in \mathcal{N}_j$ such that $\gamma(t') \in G_e$ **then**
6: Stop.
7: **end if**
8: Let $(j, j') \in \mathcal{N}_j$ such that $\gamma(t') \in G_{(j,j')}$, hence $\big(\gamma(t'), 0\big) \in S^\varepsilon_{(j,j')}$.
9: Set $x^\varepsilon(t' + \tau) = \big(\gamma(t'), \tau\big)\ \forall \tau \in [0, \varepsilon)$.
10: Set $x^\varepsilon(t' + \varepsilon) = R^\varepsilon_{(j,j')}\big(\gamma(t'), \varepsilon\big)$, $t = t' + \varepsilon$, and $j = j'$.
▷ *Note* $\big(\gamma(t'), \varepsilon\big) \overset{\widehat{R}^\varepsilon}{\sim} x^\varepsilon(t' + \varepsilon)$.
11: **end loop**

Fig. 10. Algorithm to construct a relaxed execution of a relaxation of a controlled hybrid system, $\mathcal{H}^\varepsilon$.

given execution is orbitally stable. Theorem III.2 in [30] provides one set of sufficient conditions ensuring orbital stability.

B. Relaxed Execution of a Hybrid System

Next, we define the concept of *relaxed execution* for a relaxation of a controlled hybrid system. The main idea is that, once a relaxed execution reaches a guard, we continue integrating over the strip with the relaxed vector field, f_e, as in Definition 17. Given the controlled hybrid system, $\mathcal{H}$ and its relaxation, $\mathcal{H}^\varepsilon$ for some $\varepsilon > 0$, the algorithm in Fig. 10 defines a relaxed execution of $\mathcal{H}^\varepsilon$ via construction. The resulting relaxed execution, denoted x^ε, is a continuous function defined from an interval $I \subset [0, \infty)$ to $\mathcal{M}^\varepsilon$. Note that this algorithm is only defined for initial conditions belonging to D_j for some $j \in \mathcal{J}$ since the strips are artificial objects that do not appear in $\mathcal{H}$. The generalization to all initial conditions is straighforward; we omit it to simplify the presentation.

Step 9 of the algorithm in Fig. 10 relaxes each instantaneous discrete transition by integrating over the vector field on a strip, hence forming a continuous curve on $\mathcal{M}^\varepsilon$. Also note that our definition for the relaxed execution over each strip S^ε_e, also in Step 9, is exactly equal to the maximal integral curve of f_e. Fig. 11 shows an example of a relaxed mode transition produced by the algorithm in Fig. 10. Given a hybrid system $\mathcal{H}$ and its relaxation $\mathcal{H}^\varepsilon$, the relaxed execution of $\mathcal{H}^\varepsilon$ produced by the algorithm in Fig. 10 is a delayed version of the execution of $\mathcal{H}$ produced by the algorithm in Fig. 8, since the relaxed version has to expend ε time units during each discrete transition. In that sense, our definition of relaxed execution is equivalent to an execution of a *regularized hybrid system* [8].

Note that if a relaxed execution is unique for a given initial condition and input, then the corresponding hybrid execution is also unique, but not vice versa. Indeed, consider the case of a hybrid execution performing a single discrete transition at a point, say p, where two guards intersect, i.e. $p \in G_e$ and $p \in G_{e'}$, such that $R_e(p) = R_{e'}(p)$. In this case the hybrid execution is unique, but its relaxed counterpart either evolves via S_e or $S_{e'}$, hence obtaining 2 different executions. Nevertheless, both relaxed executions reach the same point after evolving over the strip.

Next, we state our first convergence theorem.

Theorem 26. *Let $\mathcal{H}$ be a controlled hybrid system and $\mathcal{H}^\varepsilon$ be its relaxation. Let $p \in \mathcal{M}$, $u \in BV(\mathbb{R}, U)$, $x\colon I \to \mathcal{M}^\varepsilon$ be an execution of $\mathcal{H}$ with initial condition p and control u, and let $x^\varepsilon\colon I^\varepsilon \to \mathcal{M}^\varepsilon$ be a corresponding relaxed execution of x. Assume that the following conditions are satisfied:*
(1) x is orbitally stable with initial condition p and control u;

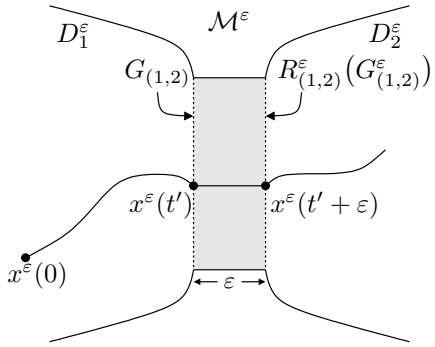

Fig. 11. Relaxed mode transition of a relaxed execution x^ε in a two–mode relaxed hybrid dynamical system.

(2) x has a finite number of discrete transitions or is a Zeno execution that accumulates; and
(3) there exists $T > 0$ such that for each ε small enough, $[0,T] \subset I \cap I^\varepsilon$ if x has a finite number of discrete transitions, and $[0,T) \subset I \cap I^\varepsilon$ if x is Zeno.

Then, $\lim_{\varepsilon\to 0} \rho^\varepsilon_{[0,T]}\big(x, x^\varepsilon\big) = 0$.

Proof. We provide the main arguments of the proof, omitting some details in the interest of brevity. First, given $j \in \mathcal{J}$ and $[\tau,\tau') \subset [0,T]$ such that $x(t) \in D_j$ for each $t \in [\tau,\tau')$, then, since $x|_{[\tau,\tau')}$ is absolutely continuous, for each $t, t' \in [\tau,\tau')$,

$$\widetilde{d}_{\mathcal{M}^\varepsilon}\big(x(t),x(t')\big) \leq L_{\widetilde{d}_{D_j}}\big(x|_{[t,t')}\big) = \int_t^{t'} \big\| f_j\big(s,x(s),u(s)\big)\big\| \,\mathrm{d}s \leq K(t'-t), \tag{18}$$

where $K = \sup\big\{ \big\| f_j\big(t,x,u\big)\big\| \mid j \in \mathcal{J},\ t \in [0,T],\ x \in \mathcal{M}^\varepsilon, u \in U\big\} < \infty$.

Second, let $k \in \mathbb{N}$ and $\{\lambda_i\}_{i=0}^k \subset [0,1]$ be a sequence such that $0 = \lambda_0 \leq \lambda_1 \leq \ldots \leq \lambda_k = 1$. Given $\varepsilon > 0$, let $\gamma_t \colon [0,1] \to \mathcal{M}^\varepsilon$ be defined by $\gamma_t(\lambda) = x^{\lambda\varepsilon}(t)$. Thus, by Theorem 21 and the algorithm in Figure 10, $\gamma_t(0) = x^0(t) = x(t)$ and $\gamma_t(1) = x^\varepsilon(t)$. Assume that $x^\varepsilon(t) \in D_j$ for each $t \in [\tau+\varepsilon, \tau'+\varepsilon)$, where $[\tau,\tau')$ is as defined above. Using Picard's Lemma (Lemma 5.6.3 in [23]), for each $t \in [\tau+\varepsilon,\tau')$,

$$\begin{aligned}
\big\|x^\varepsilon(t+\varepsilon) - x(t)\big\| &\leq e^{L(t-\tau)}\bigg(\|x^\varepsilon(\tau+\varepsilon) - x(\tau)\| + \\
&\qquad + \int_\tau^t \big\| f_j\big(s,x(s),u(s)\big) - f_j\big(s+\varepsilon,x(s),u(s+\varepsilon)\big)\big\| \,\mathrm{d}s\bigg) \\
&\leq e^{L(t-\tau)}\bigg(\|x^\varepsilon(\tau+\varepsilon) - x(\tau)\| + L\int_\tau^t \varepsilon + \|u(s) - u(s+\varepsilon)\| \,\mathrm{d}s\bigg) \\
&\leq e^{L(t-\tau)}\Big(\|x^\varepsilon(\tau+\varepsilon) - x(\tau)\| + \big(L + \mathrm{V}(u)\big)(t-\tau)\varepsilon\Big),
\end{aligned} \tag{19}$$

where we have used a standard property of the functions of bounded variation (Exercise 5.1 in [31]). Thus, if we assume that $\|x^\varepsilon(\tau+\varepsilon) - x(\tau)\| = O(\varepsilon)$, i.e. that there exists $C > 0$ such that $\|x^\varepsilon(\tau+\varepsilon) - x(\tau)\| \leq C\varepsilon$, then $\|x^\varepsilon(t+\varepsilon) - x(t)\| = O(\varepsilon)$ for each $t \in [\tau+\varepsilon,\tau')$. Using the same argument as above $\big\|x^{\lambda_{i+1}\varepsilon}(t+\varepsilon) - x^{\lambda_i\varepsilon}(t)\big\| = O((\lambda_{i+1}-\lambda_i)\varepsilon)$, which implies that γ_t is continuous for each $t \in [\tau+\varepsilon,\tau')$, and that $L(\gamma_t) = O(\varepsilon)$, hence $\widetilde{d}_{D_j}\big(x^\varepsilon(t+\varepsilon), x(t)\big) = O(\varepsilon)$.

Assuming now that x performs 2 discrete transitions at times $\tau,\tau' \in [0,T]$, such that $\tau+\varepsilon < \tau'$, transitioning from mode j to j', and the from mode j' to j''. Note that, by definition, $x|_{[0,\tau)} = x^\varepsilon|_{[0,\tau)}$. Moreover, since x is orbitally stable, we know that x^ε performs the same 2 discrete transitions for ε small enough. Let $\tau^\varepsilon + \varepsilon \in [0,T]$ be such that $x^\varepsilon(\tau^\varepsilon+\varepsilon) \in G_{(j',j'')}$. Note that $|\tau^\varepsilon - \tau'| = O(\varepsilon)$ since $x^\varepsilon \to x$ uniformly and x is Lipschitz continuous (both propositions shown above). Assume that $\tau' \leq \tau^\varepsilon + \varepsilon$ and consider the following upper bounds:

(1) If $t \in [\tau, \tau+\varepsilon)$, then $x(t) \in D_{j'}$ and $x^\varepsilon(t) \in S^\varepsilon_{(j,j')}$, thus:

$$\widetilde{d}_{\mathcal{M}^\varepsilon}\big(x(t), x^\varepsilon(t)\big) \leq \widetilde{d}_{D_{j'}}\big(x(t), x(\tau)\big) + d_{S^\varepsilon_{(j,j')}}\big(x(\tau), x^\varepsilon(t)\big) = O(\varepsilon). \tag{20}$$

(2) If $t \in [\tau+\varepsilon, \tau')$, then $x(t), x^\varepsilon(t) \in D_{j'}$, thus, using the bound obtained above:

$$\widetilde{d}_{\mathcal{M}^\varepsilon}\big(x(t), x^\varepsilon(t)\big) \leq \widetilde{d}_{D_{j'}}\big(x(t), x(t-\varepsilon)\big) + \widetilde{d}_{D_{j'}}\big(x(t-\varepsilon), x^\varepsilon(t)\big) = O(\varepsilon). \tag{21}$$

(3) If $t \in [\tau', \tau^\varepsilon+\varepsilon)$, then $x(t) \in D_{j''}$ and $x^\varepsilon \in D_{j'}$, thus, denoting $\lim_{t\uparrow\tau'} x(t) = x(\tau'_-)$:

$$\begin{aligned}\widetilde{d}_{\mathcal{M}^\varepsilon}\big(x(t), x^\varepsilon(t)\big) \leq \widetilde{d}_{D_{j''}}\big(x(t), x(\tau')\big) + d_{S^\varepsilon_{(j',j'')}}\big(x(\tau'), x(\tau'_-)\big) + \\ + \widetilde{d}_{D_{j'}}\big(x(\tau'_-), x^\varepsilon(\tau^\varepsilon+\varepsilon)\big) + \widetilde{d}_{D_{j'}}\big(x^\varepsilon(\tau^\varepsilon+\varepsilon), x^\varepsilon(t)\big) \leq O(\varepsilon).\end{aligned} \tag{22}$$

(4) If $t \in [\tau^\varepsilon+\varepsilon, \tau^\varepsilon+2\varepsilon)$, then $x(t) \in D_{j''}$ and $x^\varepsilon \in S^\varepsilon_{(j'.j'')}$, thus:

$$\widetilde{d}_{\mathcal{M}^\varepsilon}\big(x(t), x^\varepsilon(t)\big) \leq \widetilde{d}_{D_{j''}}\big(x(t), x(\tau')\big) + d_{S^\varepsilon_{(j',j'')}}\big(x(\tau'), x^\varepsilon(t)\big) \leq O(\varepsilon). \tag{23}$$

(5) If $t \in [\tau^\varepsilon+2\varepsilon, T]$, then $x(t), x^\varepsilon(t) \in D_{j''}$, thus we get the same bound as in case (2).

Therefore, $\rho^\varepsilon_{[0,T]}(x, x^\varepsilon) = O(\varepsilon)$ as desired. Note that the general case, with an arbitrary number of discrete transitions, follows by using the a similar argument as above by properly considering the time intervals and then applying the upper bounds inductively.

Next, let us consider the case when x is a Zeno execution that accumulates on p'. Let $\delta > 0$, then $x|_{[0,T-\delta]}$ has a finite number of discrete transitions, and as shown above, $\widetilde{d}_{\mathcal{M}^\varepsilon}\big(x(T-\delta), x^\varepsilon(T-\delta)\big) = O(\varepsilon)$. Moreover, $\widetilde{d}_{\mathcal{M}^\varepsilon}\big(x(T-\delta), x(t)\big) = O(\delta)$ and $\widetilde{d}_{\mathcal{M}^\varepsilon}\big(x^\varepsilon(T-\delta), x^\varepsilon(t)\big) = O(\delta)$ for each $t \in [T-\delta, T)$. The conclusion follows by noting that these bounds are valid for each $\delta > 0$. □

C. Discrete Approximations

Finally, we are able to define the *discrete approximation of a relaxed execution*, which is constructed as an extension of any existing ODE numerical integration algorithm. Given a controlled hybrid system $\mathcal{H}$, $\mathcal{A}^h_j \colon \mathbb{R} \times \mathbb{R}^{n_j} \times U \to \mathbb{R}^{n_j}$, where $h > 0$ and $j \in \mathcal{J}$, is a *numerical integrator of order* ω, if given $p \in D_j$, $u \in BV(\mathbb{R}, U)$, x the maximal integral curve of f_j with initial condition p and control u, $N = \lfloor \frac{T}{h} \rfloor$, and a sequence $\{z_k\}_{k=0}^N$ with $z_0 = p$ and $z_{k+1} = \mathcal{A}^h_j\big(kh, z_k, u(kh)\big)$, then $\sup\big\{ \|x(kh) - z_k\| \mid k \in \{0, \dots, N\}\big\} = O(h^\omega)$. This definition of numerical integrator is compatible with commonly used algorithms, including Forward and Backward Euler algorithms and the family of Runge–Kutta algorithms (Chapter 7 in [32]). The algorithm in Fig. 12 defines a discrete approximation of a relaxed execution of $\mathcal{H}^\varepsilon$. The resulting discrete approximation, for a step size $h > 0$, denoted by $z^{\varepsilon,h}$, is a function from a closed interval $I \subset [0, \infty)$ to $\mathcal{M}^\varepsilon$.

We now make several remarks about the algorithm in Fig. 12. First, the condition in Step 4 can only be satisfied, i.e. the Algorithm only stops, if $z^{\varepsilon,h}(t_k) \in \partial D_j$ and $f_j\big(t_k, z^{\varepsilon,h}(t_k), u(t_k)\big)$ is outward–pointing, since otherwise a smaller step–size would produce a valid point. Second, the function $z^{\varepsilon,h}$ is continuous on $\mathcal{M}^\varepsilon$. Third, and most importantly, similar to the algorithm in Fig. 10, the curve assigned to $z^{\varepsilon,h}$ in Step 13 is exactly the maximal integral curve of f_e while on the strip. By relaxing the guards using strips, and then endowing the strips with a trivial vector field, we avoid having to find the exact point where the trajectory intersects a guard. Our relaxation does introduce an error in the approximation, but as we show in Theorem 27, the error is of order ε. Fig. 13 shows a discrete approximation produced by the algorithm in Fig. 12 as it performs a mode transition.

Theorem 27. *Let $\mathcal{H}$ be a controlled hybrid system and $\mathcal{H}^\varepsilon$ its relaxation. Let $p \in \mathcal{M}$, $u \in BV(\mathbb{R}, U)$, and let $x \colon I \to \mathcal{M}^\varepsilon$ be a orbitally stable execution of $\mathcal{H}$ with initial condition p and control u. Furthermore, let $x^\varepsilon \colon I^\varepsilon \to \mathcal{M}^\varepsilon$ be a relaxed execution with initial condition p and control u, and let $z^{\varepsilon,h} \colon I^{\varepsilon,h} \to \mathcal{M}^\varepsilon$*

Require: $h > 0$, $k = 0$, $j \in \mathcal{J}$, and $p \in D_j$.
Set $t_0 = 0$ and $z^{\varepsilon,h}(0) = p$.
loop
  Set $n' = \inf\{n \in \mathbb{N} \mid \mathcal{A}_j^{h2^{-n}}\big(t_k, z^{\varepsilon,h}(t_k), u(t_k)\big) \in D_j^\varepsilon\}$.
  if $n' = \infty$ **then**
    return $z^{\varepsilon,h}|_{[0,t_k]}$.
  end if
  Set $t_{k+1} = t_k + h2^{-n'}$.
  Set $z^{\varepsilon,h}(t_{k+1}) = \mathcal{A}_j^{h2^{-n'}}\big(t_k, z^{\varepsilon,h}(t_k), u(t_k)\big)$.
  Set $z^{\varepsilon,h}(t) = \frac{t_{k+1}-t}{t_{k+1}-t_k} z^{\varepsilon,h}(t_k) + \frac{t-t_k}{t_{k+1}-t_k} z^{\varepsilon,h}(t_{k+1})\ \forall t \in [t_k, t_{k+1}]$.
  if $\exists (j, j') \in \mathcal{N}_j$ such that $z^{\varepsilon,h}(t_{k+1}) \in S^\varepsilon_{(j,j')}$ **then**
    Set $(q, \tau) = z^{\varepsilon,h}(t_{k+1}) \in S^\varepsilon_{(j,j')}$.
    Set $t_{k+2} = t_{k+1} + \varepsilon - \tau$.
    Set $z^{\varepsilon,h}(t) = (q, t - t_{k+1} + \tau)\ \forall t \in [t_{k+1}, t_{k+2})$.
    Set $z^{\varepsilon,h}(t_{k+2}) = R^\varepsilon_{(j,j')}(q, \varepsilon)$, $k = k + 2$, and $j = j'$.
    ▷ *Note* $(q, \varepsilon) \overset{\widehat{R}^\varepsilon}{\sim} z^{\varepsilon,h}(t_{k+2})$.
  else
    Set $k = k + 1$.
  end if
end loop

Fig. 12. Discrete approximation of a relaxed execution of the relaxation of a controlled hybrid system $\mathcal{H}^\varepsilon$.

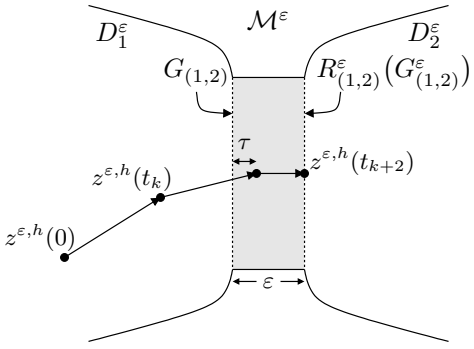

Fig. 13. Discrete approximation $z^{\varepsilon,h}$ of a relaxed execution in a two-mode hybrid dynamical system.

be its discrete approximation. If $[0, T] \subset I^\varepsilon \cap I^{\varepsilon,h}$ *for each* ε *and* h *small enough, then there exists* $C > 0$ *such that* $\lim_{h\to 0} \rho^\varepsilon_{[0,T]}\big(x^\varepsilon, z^{\varepsilon,h}\big) \leq C\varepsilon$.

Proof. As we have done with the previous proofs, we only provide a sketch of the argument in the interest of brevity. Assume that x^ε performs a single discrete transition in the interval $[0, T]$ for each ε small enough, crossing the guard $G_{(j,j')}$ at time τ^ε. Let $\delta > 0$. Since x is orbitally stable and $\mathcal{A}^h$ is convergent with order ω, for h small enough there exists an initial condition $z^{\varepsilon,h}(0)$ such that $\big|x^\varepsilon(0) - z^{\varepsilon,h}(0)\big| < \delta$ and $z^{\varepsilon,h}$ crosses the guard $G_{(j,j')}$ at time $\tau^{\varepsilon,h}_{k'} \in [t_{k'}, t_{k'+1})$ for some $k' \in \mathbb{N}$, where $\{t_k\}_{k=0}^N$ is the set of time samples associated to $z^{\varepsilon,h}$. Moreover, we can choose h small enough such that $\big|\tau^\varepsilon - t_{k'+1}\big| \leq 2\delta + O(h^\omega)$ and $\big|t_{k'+2} - \tau^\varepsilon + \varepsilon\big| = O(h^\omega)$.

Let $\sigma_m = \min\{t_{k'+1}, \tau^\varepsilon\}$, $\sigma_M = \max\{t_{k'+1}, \tau^\varepsilon\}$, $\nu_m = \min\{t_{k'+2}, \tau^\varepsilon + \varepsilon\}$, and $\nu_M = \max\{t_{k'+2}, \tau^\varepsilon + \varepsilon\}$. Also, let us assume that h is small enough such that $\sigma_M \leq \nu_m$. Then on the interval $[0, \sigma_m)$ we get convergence due to $\mathcal{A}^h$. On the interval $[\sigma_m, \sigma_M)$ one execution has transitioned into a strip, while the other is still governed by the vector field on D_j. On the interval $[\sigma_M, \omega_m)$ both executions are inside the

strip, and on the interval $[\omega_m, \omega_M)$ one execution has transitioned to a new domain, while the second is still on the strip. After time ω_M both executions are in a new domain, and we can repeat the process.

Consider the following cases:

(1) By the convergence of algorithm $\mathcal{A}^h$,

$$\widetilde{d}_{\mathcal{M}^\varepsilon}\big(x^\varepsilon(\sigma_m), z^{\varepsilon,h}(\sigma_m)\big) = O(\delta) + O(h^\omega). \tag{24}$$

(2) Using (18) from the proof of Theorem 26,

$$\widetilde{d}_{\mathcal{M}^\varepsilon}\big(x^\varepsilon(\sigma_M), z^{\varepsilon,h}(\sigma_M)\big) \leq \widetilde{d}_{\mathcal{M}^\varepsilon}\big(x^\varepsilon(\sigma_M), x^\varepsilon(\sigma_m)\big) + \widetilde{d}_{\mathcal{M}^\varepsilon}\big(x^\varepsilon(\sigma_m), z^{\varepsilon,h}(\sigma_m)\big) + \\ + \widetilde{d}_{\mathcal{M}^\varepsilon}\big(z^{\varepsilon,h}(\sigma_m), z^{\varepsilon,h}(\sigma_M)\big) = O(\delta) + O(h^\omega). \tag{25}$$

(3) Using the same argument as in the inequality above,

$$\widetilde{d}_{\mathcal{M}^\varepsilon}\big(x^\varepsilon(\nu_m), z^{\varepsilon,h}(\nu_m)\big) \leq \widetilde{d}_{\mathcal{M}^\varepsilon}\big(x^\varepsilon(\sigma_M), z^{\varepsilon,h}(\sigma_M)\big) + 2\varepsilon. \tag{26}$$

(4) Finally, again using the same argument as in case (2),

$$\widetilde{d}_{\mathcal{M}^\varepsilon}\big(x^\varepsilon(\nu_M), z^{\varepsilon,h}(\nu_M)\big) \leq \widetilde{d}_{\mathcal{M}^\varepsilon}\big(x^\varepsilon(\nu_m), z^{\varepsilon,h}(\nu_m)\big) + O(h^\omega). \tag{27}$$

The generalization to any relaxed execution defined on $\mathcal{M}^\varepsilon$ and its discrete approximation follows by noting that they perform a finite number of discrete jumps on any bounded interval and that δ can be chosen arbitrarily small. □

Next, we state the main result of this Section, which is a result of Theorems 26 and 27.

Corollary 28. *Let $\mathcal{H}$ be a hybrid dynamical system and $\mathcal{H}^\varepsilon$ be its relaxation. Let $p \in \mathcal{M}$, $u \in BV(\mathbb{R}, U)$, $x\colon I \to \mathcal{M}^\varepsilon$ be an execution of $\mathcal{H}$ with initial condition p and control u, $x^\varepsilon\colon I^\varepsilon \to \mathcal{M}^\varepsilon$ be its corresponding relaxed execution, and $z^{\varepsilon,h}\colon I^{\varepsilon,h} \to \mathcal{M}^\varepsilon$ be its corresponding discrete approximation. If the following conditions are satisfied:*

(1) x has a finite number of mode transitions or is a Zeno execution that accumulates;
(2) x is orbitally stable; and,
(3) $[0,T] \subset I \cap I^\varepsilon \cap I^{\varepsilon,h}$ for each ε and h small enough,

then $\lim_{\substack{\varepsilon\to 0\\ h\to 0}} \rho^\varepsilon_{[0,T]}\big(x, z^{\varepsilon,h}\big) = 0$.

Moreover, the rate of convergence in the $\rho^\varepsilon_{[0,T]}$–metric is $O(\varepsilon) + O(h^\omega)$.

Proof. Note that, by Theorem 26 together with the Triangle Inequality, this corollary is equivalent to proving that $\rho^\varepsilon_I\big(x^\varepsilon, z^{\varepsilon,h}\big) \to 0$ as both $\varepsilon, h \to 0$. Hence we show that $\rho^\varepsilon_I\big(x^\varepsilon, z^{\varepsilon,h}\big)$ converges uniformly on h as $\varepsilon \to 0$. Using an argument similar to the one in the proof of Theorem 7.9 in [33], proving the uniform convergence on h is equivalent to showing that $\lim_{h\to 0} \limsup_{\varepsilon\to 0} \rho^\varepsilon_I\big(x^\varepsilon, z^{\varepsilon,h}\big) = 0$, but this is true by Theorem 27, as desired.

The rate of convergence follows from the proofs of Theorems 26 and 27, in particular from inequalities (20) to (27). □

V. Examples

We apply our results in three illustrative examples: first detailing the technical advantages of our intrinsic state–space metric over trajectory–space metrics in Section V-A; subsequently comparing the performance of our provably–convergent simulation algorithm to the state–of–the–art in Section V-B; and finally applying our metric and simulation algorithm to a novel legged locomotion model in Section V-C. Each example produces executions that are orbitally stable with respect to our state–space metric; this follows from [28, Theorem 2.8.3] for the examples in Sections V-A and V-C and [9, Theorem 5.1] for the example in Section V-B.

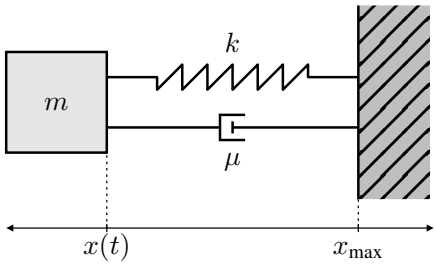

(a) Forced linear oscillator with stop.

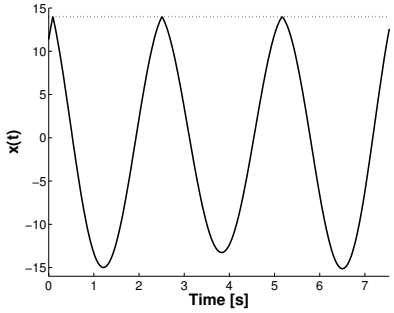

(b) Position of the analytical solution of Example 1 in Table I (solid line), and position of the stop (dotted line).

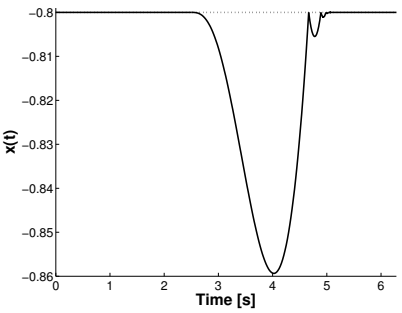

(c) Position of the analytical solution of Example 2 in Table I (solid line), and position of the stop (dotted line).

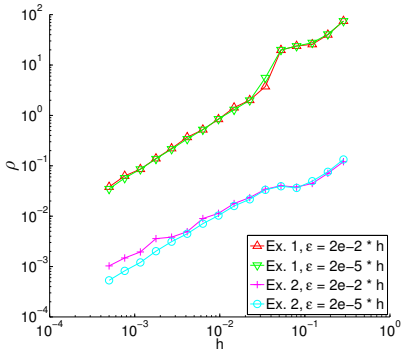

(d) $\rho^{\varepsilon}_{[0,t_{\max}]}$–error of the algorithm in Fig. 12 for the examples in Table I.

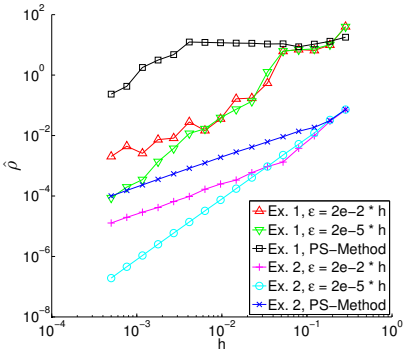

(e) $\hat{\rho}$–error of the algorithm in Fig. 12 vs. the PS Method for the examples in Table I.

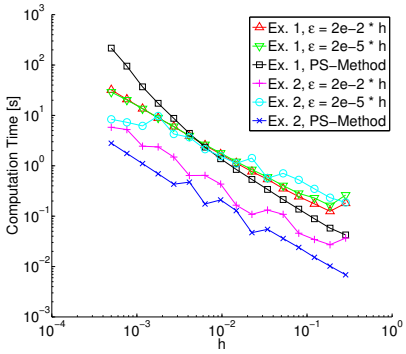

(f) Computation times of the algorithm in Fig. 12 vs. the PS Method for the examples in Table I.

Fig. 14. A mechanical system (Fig. 14a) and a pair of examples (Figs. 14b and 14c) chosen to illustrate the accuracy of the algorithm in Fig. 12 vs. the PS Method (Figs. 14d and 14e) and their computation times (Fig. 14f).

A. Metrization Example: Digital Control System

We now study the distance between executions in the digital control system of Fig. 1 using existing trajectory–space metrics and our proposed state–space metric. Consider a nominal execution $x\colon [0,T] \to D$ that crosses the two thresholds simultaneously. For each $\delta > 0$ let $y_\delta\colon [0,T] \to D$ be the execution initialized at $y_\delta(0) = x(0) + (-\delta, 0)$ and let $z_\delta\colon [0,T] \to D$ be the execution initialized at $z_\delta(0) = x(0) + (0, -\delta)$; see Fig. 1a for an illustration. For each $\delta > 0$ the executions y_δ and z_δ undergo different sequences of logical controller states, $0 \to 1 \to 3$ or $0 \to 2 \to 3$, corresponding to transitions through different discrete modes in the controlled hybrid system in Fig. 1b. In existing trajectory–space metrics [1], [2], [3], [4], y_δ and z_δ would be separated by at least unit distance. In the state–space metric we develop in Section III, the distance between y_δ and z_δ in the controlled hybrid system of Fig. 1b is equal to that between the trajectories of the discontinuous vector field in Fig. 1a, and in particular converges to zero as $\delta \to 0$.

An important consequence of this discussion is that x is orbitally stable with respect to our state–space metric, but not with respect to existing trajectory–space metrics. Therefore the algorithm described in Section IV is at present the only algorithm that yields simulations that provably converge to x.

B. Simulation Example: Forced Linear Oscillator with Stop

We consider a single degree–of–freedom oscillator consisting of a mass that is externally forced and can impact a plane fixed rigid stop, as in Fig. 14a. The state of the oscillator is the position, $x(t) \in \mathbb{R}$, and velocity, $\dot{x}(t) \in \mathbb{R}$, of the mass. The oscillator is forced with a control $u \in BV(\mathbb{R}, \mathbb{R})$. The oscillator

TABLE I
PARAMETERS USED FOR THE SIMULATIONS OF THE FORCED LINEAR OSCILLATOR WITH STOP.

	a	c	$t_{\max}$	$u(t)$	x_0	$\dot{x}_0$	$x_{\max}$	ω
Example 1	0.05	0.9	40π	$20\cos(\frac{5}{2}t)$	11.36	31.4	14	2.5
Example 2	0.95	0.5	4π	$\cos(t)$	-0.8	0	-0.8	1

is modeled as a controlled hybrid system with a single mode $D = \big\{\big(x(t), \dot{x}(t)\big) \in \mathbb{R}^2 \mid x(t) \leq x_{\max}\big\}$, and single guard corresponding to the mass impacting the stop with non–negative velocity $G = \big\{\big(x(t), \dot{x}(t)\big) \in \mathbb{R}^2 \mid x(t) = x_{\max}, \dot{x}(t) \geq 0\big\}$. Upon impact, the state is updated using the reset map $R(x, \dot{x}) = \big(x, -c\,\dot{x}\big)$, where $c \in [0, 1]$ is the coefficient of restitution. Within the single domain, the dynamics of the system are governed by $\ddot{x}(t) + 2a\dot{x}(t) + \omega^2 x(t) = m^{-1}\,u(t)$, where $\omega = \sqrt{m^{-1}k}$, $a = 0.5\,m^{-1}\,\mu$, k is the spring constant, and μ is the damping coefficient.

Given an initial condition $\big(x(t_0), \dot{x}(t_0)\big) = \big(x_0, \dot{x}_0\big) \in D$, the oscillator's motion is analytically determined by:

$$x(t) = e^{-at}\big(A_n \cos(\tilde{\omega}t) + B_n \sin(\tilde{\omega}t)\big) + \tilde{\omega}^{-1} \int_0^t u(s) e^{-a(t-s)} \sin\big(\tilde{\omega}(t-s)\big)\,\mathrm{d}s \tag{28}$$

for each $t \in [t_{n-1}, t_n)$, where $\tilde{\omega} = \sqrt{\omega^2 - a^2}$ (assuming that the damping is sub–critical), with t_n such that $x(t_n^-) = x_{\max}$ for each $n \in \mathbb{N}$, and A_n and B_n are determined by the given initial conditions when $n = 0$, or those determined by applying the reset map to $x(t_n^-)$ when $n \geq 1$. Note that determining the impact times can be done analytically. The analytical solution holds provided that the mass does not stick to the stop, since in that case the dynamics are given by $\ddot{x}(t) + 2a\dot{x}(t) + \omega^2 x(t) = m^{-1}\big(u(t) + \lambda(t)\big)$, where $\lambda(t) \in \mathbb{R}$ denotes the force generated by the stop to prevent movement. This equation holds as long as $x(t) = x_{\max}$, $\dot{x}(t) = \ddot{x}(t) = 0$, and the reaction of the stop is negative, i.e. $\lambda(t) \geq m\,\omega^2\,x_{\max}$. For the contact to cease, $\lambda(t) - m\,\omega^2\,x_{\max}$ must become zero and change sign. Once this happens, the analytical solution can be used again to construct the motion of the mass with the initial condition $(x_{\max}, 0)$.

Assuming that the forcing u is continuous (an assumption that is violated by many control schemes such as ones generated via optimal control) a convergent numerical simulation scheme, which we call the PS Method, to determine the position of a mechanical system with unilateral constraints was proposed in [16]. Given a step–size $h > 0$ and $t_k = t_0 + h\,k$ for each $k \in \mathbb{N}$, their approach is a two–step method that computes a set of positions, $z_{\text{PS}} \colon \{t_k\}_{k\in\mathbb{N}} \to \mathbb{R}$, by $z_{\text{PS}}(t_0) = x_0$ and:

$$\begin{aligned} z_{\text{PS}}(t_1) &= x_0 + \dot{x}_0 h + \frac{h^2}{2}\big(u(0) - 2a\dot{x}_0 - \omega^2 x_0\big), \\ z_{\text{PS}}(t_{k+1}) &= -c\,z_{\text{PS}}(t_{k-1}) + \min\big\{y_{\text{PS}}(t_k), (1+c)x_{\max}\big\}, \\ y_{\text{PS}}(t_k) &= \frac{1}{1+ah}\Big(h^2 u(t_k) + (2 - h^2\omega^2) z_{\text{PS}}(t_k) - \big((1-c) - (1+c)a\,h\big) z_{\text{PS}}(t_{k-1})\Big). \end{aligned} \tag{29}$$

We illustrate the performance of our approach by considering the two examples described in Table I whose solutions, which are defined for all $t \in [0, t_{\max}]$, can be computed analytically. The position component of the analytical trajectory of each example is plotted in Figs. 14b and 14c. The evaluation of the performance of our algorithm as described in Fig. 12 using ρ^ε, as in Definition 22, is shown in Fig. 14d. To make our approach comparable to the PS Method, for $\mathcal{A}^h$ we use a Runge–Kutta of order two which is called the midpoint method. We cannot use ρ^ε to compare our discrete approximation algorithm to the PS method since the PS method does not compute the velocities of the hybrid system. Hence, we use the evaluation metric proposed in [34] which compares a numerically simulated position trajectory, $z_{\text{pos}} \colon \{t_k\}_{k\in\mathbb{N}} \to \mathbb{R}$, to the analytically computed position trajectory, $x_{\text{analytic}} \colon [0, t_{\max}] \to \mathbb{R}$, at the sample points $\{t_k\}_{k\in\mathbb{N}} \cap [0, t_{\max}]$ as follows:

$$\hat{\rho}(z_{\text{pos}}, x_{\text{analytic}}) = \max\big\{|z_{\text{pos}}(t_k) - x_{\text{analytic}}(t_k)| \;\big|\; \{t_k\}_{k\in\mathbb{N}} \cap [0, t_{\max}]\big\}. \tag{30}$$

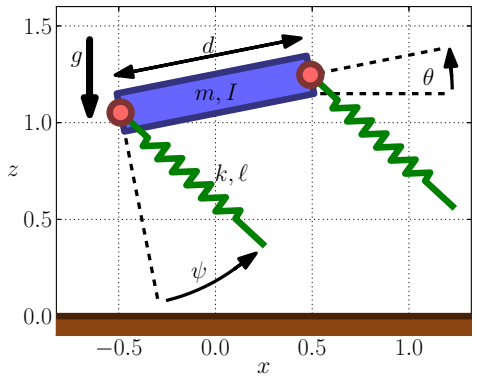

Fig. 15. Schematic for the saggital–plane locomotion model with three mechanical degrees of freedom.

The result of this comparison is illustrated in Fig. 14e. Finally, the computation time on a 32 GB, 3.1 GHz *Xeon* processor computer for each of the examples as a function of the step–size and relaxation parameter is shown in Fig. 14f. Notice in particular that we are able to achieve higher accuracy with respect to the $\hat{\rho}$ evaluation metric at much faster speeds. In Example 1, for step–sizes $h \leq 10^{-1}$, our numerical simulation method is consistently more accurate by several orders of magnitude and generally several orders of magnitude faster than the PS method. In Example 2, using a step–size of approximately $h = 10^{-2}$ and relaxation parameter $\varepsilon = 2 \cdot 10^{-7}$, our numerical simulation achieves a $\hat{\rho}$ value of approximately 10^{-4} while taking approximately 0.1 seconds, whereas the PS method requires a step–size of $h = 5 \cdot 10^{-4}$ which takes approximately 5 seconds in order to achieve the same level of accuracy.

C. Simultaneous Transitions in Models of Legged Locomotion

As a terrestrial agent traverses an environment, its appendages intermittently contact the terrain. Since the equations governing the agent's motion change with each limb contact, the dynamics are naturally modeled by a controlled hybrid system with discrete modes corresponding to distinct contact configurations. Because the dynamics of dexterous manipulation are equivalent to that of legged locomotion [35], such controlled hybrid systems model a broad and important class of dynamic interactions between an agent and its environment.

Legged animals commonly utilize gaits that, on average, involve the simultaneous transition of multiple limbs from aerial motion to ground contact [36], [37]. Similarly, many multi–legged robots enforce simultaneous leg touchdown via virtual constraints implemented algorithmically [38], [39] or physical constraints implemented kinematically [40], [41]. Trajectories modeling such gaits pass through the intersection of multiple transition surfaces in the corresponding controlled hybrid system models. Therefore simulation of this frequently–observed behavior requires a numerical integration scheme that can accommodate overlapping guards. The algorithm in Fig. 12 has this capability, and to the best of our knowledge is the only existing algorithm possessing this property. We demonstrate this advanced capability using a *pronking* gait in a saggital–plane locomotion model.

Fig. 15 contains an extension of the "Passive RHex–runner" in [42] that allows pitching motion. A rigid body with mass m and moment–of–inertia I moves in the saggital plane under the influence of gravity g. Linear leg–springs are attached to the body via a frictionless pin joint located symmetrically at distance $d/2$ from the center–of–mass. The leg–springs are massless with linear stiffness k, rest length ℓ, and make an angle ψ with respect to the body while in the air. When a foot touches the ground it attaches via a frictionless pin joint, and it detaches when the leg extends to its rest length.

A *pronk* is a gait wherein all legs touch down and lift off from the ground at the same time [36], [37]. Due to symmetries in our model, motion with pitch angle $\theta = 0$ for all time is invariant. Therefore periodic orbits for the *spring–loaded inverted pendulum* model in [43] correspond exactly to pronking gaits for

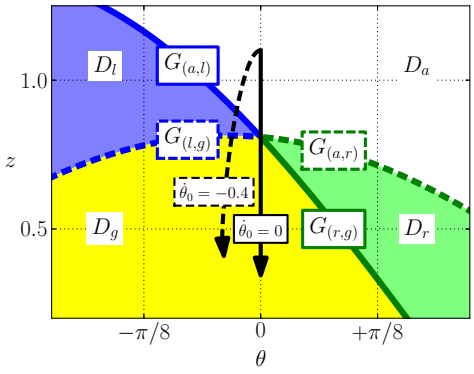

Fig. 16. Projection of guards in (θ, z) coordinates for transition from aerial domain D_a to ground domain D_g with parameters $d = \ell = 1$, $\psi = \pi/5$.

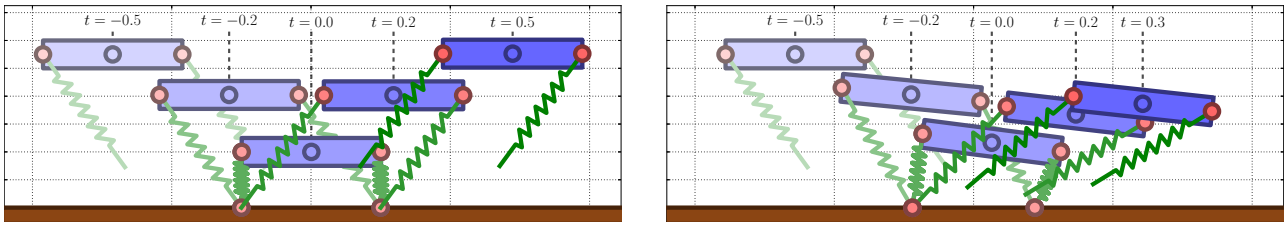

Fig. 17. Snapshots of *pronk* at discrete transition times from initial condition $(x_0, z_0, \theta_0, \dot{x}_0, \dot{z}_0, \dot{\theta}_0) = (0, 1.1, 0, 3.4, 0, 0)$, parameters $(m, I, k, \ell, d, g, \psi) = (1, 1, 30, 1, 1, 9.81, \pi/5)$, step size $h = 10^{-3}$, relaxation parameter $\varepsilon = 10^{-2}$ (left). Same as before, but with $\dot{\theta}_0 = -0.4$ (right).

our model. Fig. 16 contains a projection of the guards $G_{(a,l)}$, $G_{(a,r)}$, $G_{(l,g)}$, $G_{(r,g)}$ in (θ, z) coordinates for the transition from the aerial domain D_a to the ground domain D_g through left stance D_l and right stance D_r. The pronking trajectory is illustrated by a downward–pointing vertical arrow, and a nearby trajectory initialized with negative rotational velocity is illustrated by a dashed line. Fig. 17 contains snapshots from these simulations.

The $\dot{\theta}_0 = 0$ trajectory in Fig. 16 clearly demonstrates the need for a simulation algorithm that allows the intersection of multiple transition surfaces. We emphasize that our state–space metric was necessary to derive a convergent numerical approximation for this execution: since the discrete mode sequence differs for any pair of trajectories arbitrarily close to the $\dot{\theta}_0 = 0$ execution that pass through the interior of D_l and D_r, respectively, application of existing trajectory–space metrics [1], [3], [4] would yield a distance larger than unity between the pair. Consequently, to the best of our knowledge, no existing provably–convergent numerical simulation algorithm based on a trajectory–space metric is applicable to the $\dot{\theta}_0 = 0$ execution.

Another interesting property of this example is that it is possible to show (by carefully studying the transitions between vector fields through the guards) that the hybrid quotient space $\mathcal{M}$ is a smooth 6–dimensional manifold near the *pronk* execution, and that the piecewise–defined dynamics yield a continuously–differentiable vector field on this quotient.

VI. Conclusion

We developed an algorithm for the numerical simulation of controlled hybrid systems and proved the uniform convergence of our approximations to executions using a novel metrization of the controlled hybrid system's state space. The metric and the algorithm impose minimal assumptions on the hybrid system beyond those required to guarantee existence and uniqueness of executions. As a consequence, our algorithm does not require a specialized mechanism to handle overlapping guards or control inputs: a single code (freely available at `http://purl.org/sburden/hssim`) will accurately simulate any orbitally stable execution of the hybrid system under investigation. Beyond their immediate utility, it is our conviction

that these tools provide a foundation for formal analysis and computational controller synthesis in hybrid systems.

REFERENCES

[1] L. Tavernini, "Differential automata and their discrete simulators," *Nonlinear Analysis: Theory, Methods & Applications*, vol. 11, no. 6, pp. 665–683, 1987.

[2] D. Gokhman, "Topologies for hybrid solutions," *Nonlinear Analysis: Hybrid Systems*, vol. 2, no. 2, pp. 468–473, 2008.

[3] L. Tavernini, "Generic asymptotic error estimates for the numerical simulation of hybrid systems," *Nonlinear Analysis: Hybrid Systems*, vol. 3, no. 2, pp. 108–123, 2009.

[4] R. G. Sanfelice and A. R. Teel, "Dynamical properties of hybrid systems simulators," *Automatica*, vol. 46, no. 2, pp. 239–248, 2010.

[5] A. Nerode and W. Kohn, "Models for hybrid systems: Automata, topologies, controllability, observability," in *Proceedings of the Workshop on the Theory of Hybrid Systems*, 1993, pp. 317–356.

[6] S. N. Simic, K. H. Johansson, J. Lygeros, and S. S. Sastry, "Towards a geometric theory of hybrid systems," *Dynamics of Continuous Discrete and Impulsive Systems Series B: Applications & Algorithms*, vol. 12, no. 5/6, pp. 649–688, 2005.

[7] A. D. Ames and S. S. Sastry, "A homology theory for hybrid systems: Hybrid homology," in *Proceedings of the 8th International Workshop on Hybrid Systems: Computation and Control*, 2005, pp. 86–102.

[8] K. H. Johansson, M. Egerstedt, J. Lygeros, and S. S. Sastry, "On the regularization of Zeno hybrid automata," *Systems & Control Letters*, vol. 38, no. 3, pp. 141–150, 1999.

[9] M. Schatzman, "Uniqueness and continuous dependence on data for one–dimensional impact problems," *Mathematical and Computer Modelling*, vol. 28, no. 4—8, pp. 1–18, 1998.

[10] R. Goebel and A. R. Teel, "Solutions to hybrid inclusions via set and graphical convergence with stability theory applications," *Automatica*, vol. 42, no. 4, pp. 573–587, 2006.

[11] D. Pollard, *Convergence of Stochastic Processes*, ser. Springer Series in Statistics. Springer, 1984.

[12] M. Carver, "Efficient integration over discontinuities in ordinary differential equation simulations," *Mathematics and Computers in Simulation*, vol. 20, no. 3, pp. 190–196, 1978.

[13] L. F. Shampine, I. Gladwell, and R. W. Brankin, "Reliable solution of special problems for ODEs," *ACM Transactions on Mathematical Software*, vol. 17, no. 1, pp. 11–25, 1991.

[14] J. Guckenheimer and A. Nerode, "Simulation for hybrid systems and nonlinear control," in *Proceedings of the 31st IEEE Conference on Decision and Control*, 1992, pp. 2980–2981.

[15] J. Esposito, V. Kumar, and G. J. Pappas, "Accurate event detection for simulating hybrid systems," in *Proceedings of the 4th International Workshop on Hybrid Systems: Computation and Control*, 2001, pp. 204–217.

[16] L. Paoli and M. Schatzman, "A numerical scheme for impact problems II: The multidimensional case," *SIAM journal on numerical analysis*, vol. 40, no. 2, pp. 734–768, 2003.

[17] S. Burden, H. Gonzalez, R. Vasudevan, R. Bajcsy, and S. S. Sastry, "Numerical integration of hybrid dynamical systems via domain relaxation," in *Proceedings of the 50th IEEE Conference on Decision and Control*, 2011, pp. 3958–3965.

[18] J. L. Kelley, *General Topology*, ser. Graduate Texts in Mathematics. Springer, 1955.

[19] J. Munkres, *Topology*. Prentice–Hall, 2000.

[20] J. L. Hein, *Discrete Structures, Logic, and Computability*, 3rd ed. Jones & Bartlett Learning, 2009.

[21] D. Burago, Y. Burago, and S. Ivanov, *A Course in Metric Geometry*, ser. Graduate Studies in Mathematics. American Mathematical Society, 2001.

[22] E. J. McShane, "Extension of range of functions," *Bulletin of the American Mathematical Society*, vol. 40, no. 12, pp. 837–843, 1934.

[23] E. Polak, *Optimization: Algorithms and Consistent Approximation*, ser. Applied Mathematical Sciences. Springer, 1997.

[24] G. Folland, *Real Analysis: Modern Techniques and Their Applications*, 2nd ed., ser. Pure and Applied Mathematics. John Wiley & Sons, 1999.

[25] J. M. Lee, *Introduction to Smooth Manifolds*, ser. Graduate Texts in Mathematics. Springer, 2003.

[26] C. Cai, R. Goebel, and A. R. Teel, "Relaxation results for hybrid inclusions," *Set-Valued Analysis*, vol. 16, pp. 733–757, 2008.

[27] V. I. Utkin, "Variable structure systems with sliding modes," *IEEE Transactions on Automatic Control*, vol. 22, no. 2, pp. 212–222, 1977.

[28] A. F. Filippov, *Differential Equations with Discontinuous Righthand Sides*. Kluwer Academic Publishers, 1988.

[29] J. Zhang, K. H. Johansson, J. Lygeros, and S. S. Sastry, "Zeno hybrid systems," *International Journal of Robust and Nonlinear Control*, vol. 11, no. 5, pp. 435–451, 2001.

[30] J. Lygeros, K. H. Johansson, S. N. Simic, J. Zhang, and S. S. Sastry, "Dynamical properties of hybrid automata," *IEEE Transactions on Automatic Control*, vol. 48, no. 1, pp. 2–17, 2003.

[31] W. P. Ziemer, *Weakly Differentiable Functions*, ser. Graduate Texts in Mathematics. Springer, 1989.

[32] R. LeVeque, *Finite Difference Methods for Ordinary and Partial Differential Equations: Steady–State and Time–Dependent Problems*, ser. Classics in Applied Mathematics. Society for Industrial and Applied Mathematics, 2007.

[33] W. Rudin, *Principles of Mathematical Analysis*. McGraw–Hill, 1964.

[34] O. Janin and C. Lamarque, "Comparison of several numerical methods for mechanical systems with impacts," *International Journal for Numerical Methods in Engineering*, vol. 51, no. 9, pp. 1101–1132, 2001.

[35] A. M. Johnson and D. E. Koditschek, "Legged self–manipulation," *IEEE Access*, vol. 1, pp. 310–334, 2013.

[36] R. M. Alexander, "The gaits of bipedal and quadrupedal animals," *The International Journal of Robotics Research*, vol. 3, no. 2, pp. 49–59, 1984.

[37] M. Golubitsky, I. Stewart, P. L. Buono, and J. J. Collins, "Symmetry in locomotor central pattern generators and animal gaits," *Nature*, vol. 401, no. 6754, pp. 693–695, 1999.

[38] M. Raibert, M. Chepponis, and H. Brown Jr., "Running on four legs as though they were one," *IEEE Journal of Robotics and Automation*, vol. 2, no. 2, pp. 70–82, 1986.

[39] U. Saranli, M. Buehler, and D. E. Koditschek, "RHex: A simple and highly mobile hexapod robot," *The International Journal of Robotics Research*, vol. 20, no. 7, pp. 616–631, 2001.

[40] S. Kim, J. Clark, and M. Cutkosky, "iSprawl: Design and tuning for high–speed autonomous open–loop running," *The International Journal of Robotics Research*, vol. 25, no. 9, pp. 903–912, 2006.

[41] A. Hoover, S. Burden, X. Fu, S. S. Sastry, and R. Fearing, "Bio–inspired design and dynamic maneuverability of a minimally actuated six–legged robot," in *Proceedings of the 3rd IEEE International Conference on Biomedical Robotics and Biomechatronics*, 2010, pp. 869–876.

[42] J. Seipel and P. Holmes, "Three–dimensional translational dynamics and stability of multi–legged runners," *The International Journal of Robotics Research*, vol. 25, no. 9, pp. 889–902, 2006.

[43] R. M. Ghigliazza, R. Altendorfer, P. Holmes, and D. E. Koditschek, "A simply stabilized running model," *SIAM Journal on Applied Dynamical Systems*, vol. 2, no. 2, pp. 187–218, 2003.